2006

# Slo3 K+ channels: Voltage and pH dependence of macroscopic currents

Xue Zhang
*Washington University School of Medicine in St. Louis*

Xuhui Zeng
*Washington University School of Medicine in St. Louis*

Christopher J. Lingle
*Washington University School of Medicine in St. Louis*

Published August 28, 2006



# Slo3 $K^+$ Channels: Voltage and pH Dependence of Macroscopic Currents

Xue Zhang, Xuhui Zeng, and Christopher J. Lingle

Department of Anesthesiology and Department of Anatomy and Neurobiology, Washington University School of Medicine, St. Louis, MO 63110

The mouse *Slo3* gene (KCNMA3) encodes a $K^+$ channel that is regulated by changes in cytosolic pH. Like Slo1 subunits responsible for the $Ca^{2+}$ and voltage-activated BK-type channel, the Slo3 α subunit contains a pore module with homology to voltage-gated $K^+$ channels and also an extensive cytosolic C terminus thought to be responsible for ligand dependence. For the Slo3 $K^+$ channel, increases in cytosolic pH promote channel activation, but very little is known about many fundamental properties of Slo3 currents. Here we define the dependence of macroscopic conductance on voltage and pH and, in particular, examine Slo3 conductance activated at negative potentials. Using this information, the ability of a Horrigan-Aldrich–type of general allosteric model to account for Slo3 gating is examined. Finally, the pH and voltage dependence of Slo3 activation and deactivation kinetics is reported. The results indicate that Slo3 differs from Slo1 in several important ways. The limiting conductance activated at the most positive potentials exhibits a pH-dependent maximum, suggesting differences in the limiting open probability at different pH. Furthermore, over a 600 mV range of voltages (−300 to +300 mV), Slo3 conductance shifts only about two to three orders of magnitude, and the limiting conductance at negative potentials is relatively voltage independent compared to Slo1. Within the context of the Horrigan-Aldrich model, these results indicate that the intrinsic voltage dependence ($z_L$) of the Slo3 closed–open equilibrium and the coupling ($D$) between voltage sensor movement are less than in Slo1. The kinetic behavior of Slo3 currents also differs markedly from Slo1. Both activation and deactivation are best described by two exponential components, both of which are only weakly voltage dependent. Qualitatively, the properties of the two kinetic components in the activation time course suggest that increases in pH increase the fraction of more rapidly opening channels.

## INTRODUCTION

$K^+$ channels formed from α subunits encoded by the *Slo* gene family (Adelman et al., 1992; Butler et al., 1993) are characterized by a large cytosolic C-terminal structure that is thought to be involved in ligand-dependent regulation of the channels (Wei et al., 1994; Schreiber and Salkoff, 1997; Schreiber et al., 1998; Bhattacharjee et al., 2002; Jiang et al., 2002; Shi et al., 2002; Xia et al., 2002; Bhattacharjee et al., 2003; Yuan et al., 2003; Xia et al., 2004). In fact, the hallmark for each member of the Slo family appears to be regulation by a specific cytosolic ligand, $Ca^{2+}$ for Slo1 (Wei et al., 1994; Schreiber and Salkoff, 1997), $Na^+$ for both Slo2.1 (Slick) and Slo2.2 (Slack) (Bhattacharjee et al., 2002; Bhattacharjee et al., 2003; Yuan et al., 2003), and pH for Slo3 (Schreiber et al., 1998; Xia et al., 2004). The most well-known member of this channel family is the Slo1 or BK channel, a large-conductance, $Ca^{2+}$- and voltage-dependent $K^+$ channel (Barrett et al., 1982). The large single channel conductance of the BK channel and its regulation by two physiological signals have made it a model channel for detailed investigation of channel function (McManus and Magleby, 1991), but much less is known about the other Slo family members. Among the less well-studied Slo family members, Slo3 shares the most extensive sequence homology with Slo1 (Schreiber et al., 1998). In contrast to Slo1, Slo3 is insensitive to cytosolic $Ca^{2+}$ and appears sensitive to cytosolic pH (Schreiber et al., 1998; Xia et al., 2004). In contrast to the wide distribution of channels arising from either Slo1 and Slo2.x subunits, Slo3 has a much more limited pattern of expression than the other family members, being found predominantly in mouse testis (Schreiber et al., 1998). Although Slo3 was first cloned over 5 years ago, information about its functional properties remains rather limited.

Mouse Slo3 channels are $K^+$ channels reported to have a single channel conductance of ∼90 pS (Schreiber et al., 1998). In the original report (Schreiber et al., 1998), channel activity was increased by membrane depolarization, consistent with the presence of a voltage sensor segment characteristic of voltage-dependent $K^+$ channels. In addition, channel activity was also increased by elevations in pH; increasing $Ca^{2+}$ from 0 to 100 μM had no obvious effect on mSlo3 channel openings. Other inferences about Slo3 properties have come from chimeric constructs, in which portions of the C terminus of Slo1 are replaced with the

Correspondence to Chris Lingle: clingle@morpheus.wustl.edu

Abbreviations used in this paper: BK, large conductance $Ca^{2+}$-activated $K^+$; DEPC, diethylpyrocarbonate.

Published August 28, 2006

corresponding segments from Slo3. In general, such observations have supported the view that Slo3 lacks the sites necessary for $Ca^{2+}$-dependent regulation that is characteristic of Slo1 (Moss and Magleby, 2001; Qian et al., 2002; Shi et al., 2002; Xia et al., 2004), but have provided little insight into how pH and voltage may regulate Slo3 activity.

Here we provide a more detailed examination of the basic functional properties of mSlo3 macroscopic current after heterologous expression in *Xenopus* oocytes. The results identify a number of major differences in Slo3 channel function from that of Slo1 that ultimately may provide insight into the functional roles of specific structural elements within this channel family. The results support the view that, in addition to the identity and effect of the regulatory ligand, Slo1 and Slo3 differ in two primary ways: first, the intrinsic voltage dependence of the Slo3 closed–open equilibrium is weaker, and, second, voltage sensor movement in Slo3 is much more weakly coupled to channel opening. A potentially physiological important consequence of these differences is that appreciable activation of Slo3 current can occur at potentials negative to 0 in response to elevations of cytosolic pH.

## MATERIALS AND METHODS

### Oocyte Removal and Culture

The procedures for preparation and injection of stage IV *Xenopus laevis* oocytes followed those used previously in this lab (Xia et al., 1999, 2002). mSlo3 cRNA (~1 ng/ml with no dilution) was typically injected at a volume of ~40 nl. To obtain relatively substantial currents, oocytes were used at times up to 14 d after injection. As a comparison, injection of 1:20 dilutions of mSlo1 RNA yield currents of comparable magnitude within ~3 d after injection.

### Chimeric Constructs and Mutations

The mSlo3 construct (Schreiber et al., 1998) obtained from L. Salkoff (Washington University School of Medicine) was modified as previously described (Xia et al., 2004). The accession number containing updated information regarding Slo3 is AF039213.

### Recording Pipettes

Patch clamp recording pipettes were made from borosilicate capillary tubes (Drummond Microcaps, 100 μl). To increase the amplitude of Slo3 currents in a patch, tip diameters in excess of 1 μ were frequently employed, resulting in pipette resistances of <1 MΩ. Pipette tips were coated with Sylgard (Sylgard 184, Dow Chemical Corp.) and then fire polished.

### Electrophysiology

All currents were recorded in the inside-out configuration (Hamill et al., 1981) using an Axopatch 200 amplifier (Molecular Devices) and the Clampex program from the pClamp software package (Molecular Devices).

Gigaohm seals were formed in frog Ringer (in mM, 115 NaCl, 2.5 KCl, 1.8 $CaCl_2$, 10 HEPES, pH 7.4). Excised patches were moved into flowing test solutions bathing the cytosolic membrane face. The standard pipette/extracellular solution was (in mM) 140 K-methanesulfonate, 20 KOH, 10 HEPES, 2 $MgCl_2$, pH 7.0. The composition of solutions bathing the cytoplasmic face of the patch membrane contained (in mM) 140 K-methanesulfonate, 20 KOH, 10 HEPES, and 5 EGTA at pH 7.0.

Procedures for solution application were as employed previously (Herrington et al., 1995; Zeng et al., 2001). A perfusion pipette with 100–200 μ tip was packed with 7 PE10 tubes. Each tube was under separate valve control, and solution flowed continuously from only one PE10 tube at a time onto the excised patch. All experiments were at room temperature (~22–25°C). Salts for solution preparation were obtained from Sigma-Aldrich.

### Data Analysis

Analysis of current recordings was accomplished either with Clampfit (Molecular Devices) or with programs written in this laboratory. $G/V$ curves were generally constructed from measurements of steady-state current, although in some cases from tail currents measured 100–200 μs after repolarization. For families of $G/V$ curves obtained within a patch, conductances were normalized to estimates of maximal conductance obtained at pH 9.0. Individual $G/V$ curves were fit with a Boltzmann function of the following form:

$$G(V) = \frac{G_{\max}}{1 + \exp^{\frac{-zF(V-V_h)}{RT}}}, \quad (1)$$

where $G_{\max}$ is the fitted value for maximal conductance at a given pH, $V_h$ is the voltage of half maximal activation of conductance, and $z$ reflects the net charge moved across the membrane during the transition from the closed to the open state.

To characterize tail currents associated with rapid deactivation, currents were sampled at either 5- or 20-μs intervals. Filtering by the amplifier during data acquisition was at either 10 or 50 kHz. Because of appreciable Slo3 current activation at potentials negative to −100 mV at pH of 7.4 and higher, currents were obtained without leak subtraction. In general, we have focused on patches in which Slo3 currents were sufficiently large that capacity transients contribute only minimally to the observed currents. In some cases, in order to examine early components of either activation or deactivation, we employed a subtraction procedure in which the scaled current elicited by a step to 0 mV was subtracted from a given test sweep, thereby removing linear uncompensated slow and fast components of capacitance.

Amplitude ratios for slow and fast components of current relaxation were determined from extrapolation of the fitted two component relaxations to a time point 40 μs after the nominal onset of the voltage step. Typically, three to six sweeps were averaged to generate traces used for analysis of activation time course. Despite the averaging, stochastic variability among traces resulted in considerable scatter in estimates of the time constants.

### Allosteric Models of Activation of BK Channels

The $Ca^{2+}$ and voltage dependence of activation of the Slo1 BK channels can be reasonably well described by allosteric models in which $Ca^{2+}$ and voltage both regulate a closed (C) to open (O) conformational change (Cui et al., 1997; Rothberg and Magleby, 1999; Rothberg and Magleby, 2000; Horrigan and Aldrich, 2002). Thus, a $Ca^{2+}$-dependent mechanism couples to channel opening in a relatively independent fashion from the coupling of voltage sensor movement to channel opening. In the case of Slo1, only a small amount of direct coupling between the $Ca^{2+}$-sensing mechanism and the voltage sensor is observed (Horrigan and Aldrich, 2002). Here, we assess whether this same general scheme can account for the pH-dependent regulation of Slo3 channel gating. For the scheme used here, we assume that the effects of pH involve a single pH-dependent equilibrium occurring on each of four subunits. The system is described by three characteristic

Published August 28, 2006

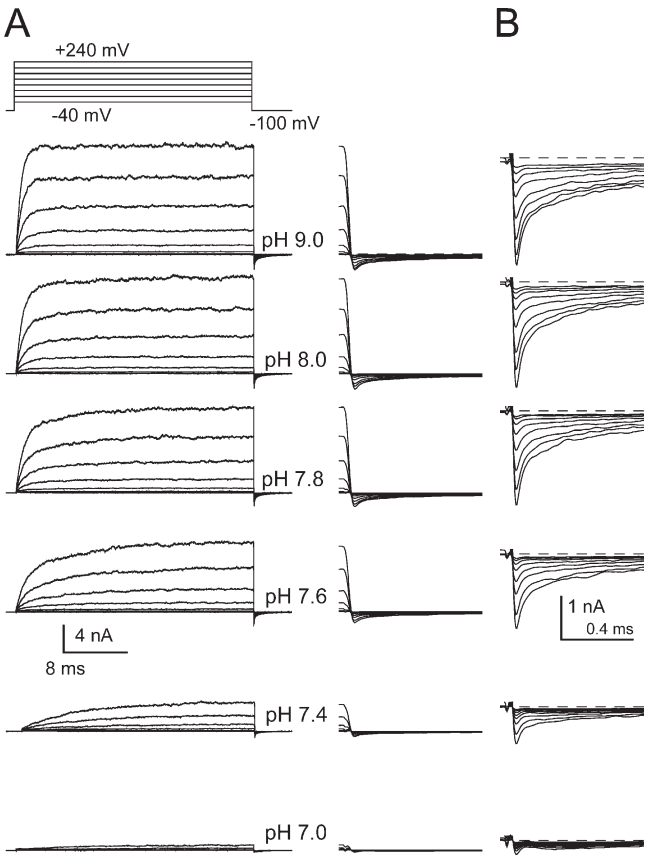


**Figure 1.** Increases in pH result in increased Slo3 current activation. (A) An inside-out patch expressing Slo3 channels was bathed with 0 $Ca^{2+}$ solutions with pH set to the indicated nominal values. Patches were activated by the indicated voltage protocol. Minimal current activation is observed with pH 7.0 even at +240 mV. Increases in pH result in faster and more robust current activation. (B) Tail currents from the panels in A are shown on a faster time base on the left and with larger amplification on the right. Note that even at the highest pH, the tail currents do not exhibit saturation in activation of conductance.

equilibrium constants: *L* defines the intrinsic equilibrium constant for the C-O transition; *J* defines the equilibrium constant for the voltage sensor movement (in the nonprotonated condition); and *K* defines the equilibrium constant for interaction with a proton. In turn, each process is allosterically coupled to the other two processes by coupling constants. *D* defines the coupling between voltage sensor movement and channel opening; *C* defines the coupling between pH and channel opening; *E* defines the coupling between pH and voltage sensor movement. These relationships are encapsulated in the following scheme:

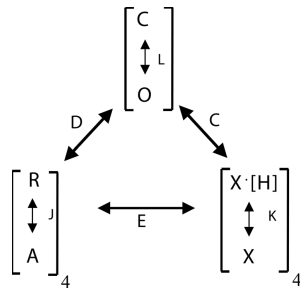


(Scheme 1)

The overall equilibrium predictions for channel open probability based on this gating scheme are given by:

$$P(V,[H]) = \frac{L(1+KC+JD+KCJDE)^4}{L(1+KC+JD+KCJDE)^4+(1+K+J+KJE)^4} \quad (2)$$

$$P(V,[H]) = \frac{1}{1+\frac{1}{L}\left[\frac{1+K+J+KJE}{(1+KC+JD+KCJDE)}\right]^4}, \quad (3)$$

where $L = L(0)*\exp(z_L V/kT)$, $J = J(0)*\exp(z_J V/kT)$, and $K = [H^+]/K_d$ where $K_d$ is the pK for the protonable group.

For Slo1 it has proven possible to define specific experimental conditions in which gating behavior is controlled by a reduced gating model, thereby defining a limited set of allosteric parameters (Horrigan and Aldrich, 2002; Ma et al., 2006). This strategy has allowed robust estimation of the allosteric constants defining regulation of Slo1 gating. Various aspects of Slo3 currents make it technically more difficult or even impractical to define independently more than a subset of the important parameters. Therefore, the aim of this work is twofold: first, to assess whether a model of this type is consistent with experimental observations and, second, based on parameters that can be reasonably well defined, to ask whether similarities and differences between Slo1 and Slo3 can be accounted for by any of the parameters.

## RESULTS

### The pH Dependence of mSlo3 Currents

Macroscopic currents resulting from expression of *mSlo3* cRNA in *Xenopus* oocytes are illustrated in Fig. 1. At pH 7.0, voltage steps as positive as +240 mV produce only a small fractional activation of current, while a marked increase in current activation is observed with increases in pH over the range of pH 7.4 through pH 9.0. As pH is increased, currents at a given voltage are more rapidly activated.

An interesting property of the Slo3 currents is the small amplitude and rapid deactivation of tail currents after repolarization (Fig. 1 B). At symmetric voltages, the maximal detectable tail current amplitude is markedly reduced relative to the current at positive potentials (see below). Because of the small size and rapidity of the inward current tails, conductance–voltage (*G/V*) curves at each pH (Fig. 2 A) were typically generated from the peak outward currents recorded at each activation potential. Within each patch, conductances under any condition were normalized to the maximal conductance recorded for the full set of measurements over all pH. An increase in pH allows Slo3 current to be activated at more negative voltages (Fig. 2 A) and there is the beginning of some saturation in *G/V* curves as pH approaches 8.5. We also observed additional shifts in gating when pH is increased to 9.5 (unpublished data), but such shifts appeared to be somewhat irreversible

Published August 28, 2006

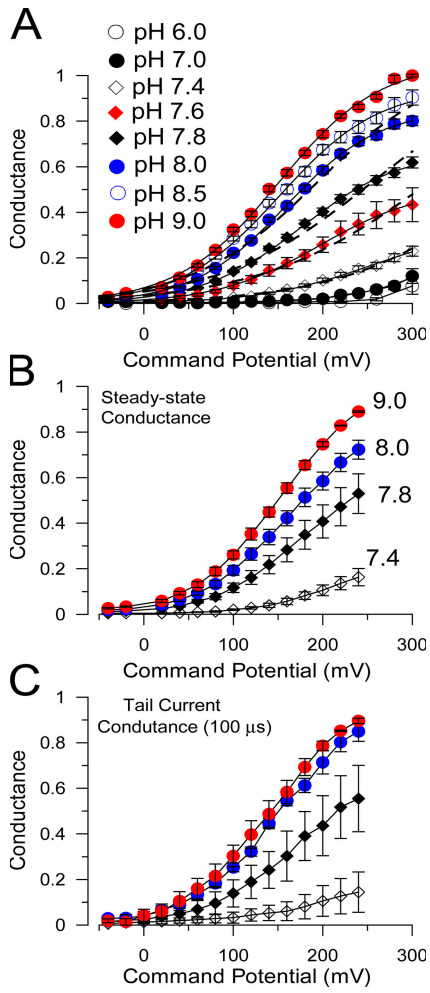


**Figure 2.** pH dependence of Slo3 macroscopic conductance. In A, steady-state currents were measured from records as in Fig. 1 and converted to conductances. For results from any individual patch, $G/V$ curves were normalized to the maximal conductance observed with pH 9.0. The full set of pH was not tested on all patches, but each point is the mean of 4–18 patches. In B and C, macroscopic conductance was determined both from steady-state currents (B) or tail currents (C) for a set of four patches at pH of 7.4, 7.8, 8.0, and 9.0. For tail current $G/V$s a single current value at 100 µs after the nominal onset of the voltage step was used.

and patch stability was a problem above pH 9.0. A limiting $G/V$ curve at low pH could not be defined even with voltage steps to +300 mV. For a limited set of patches with more robust outward currents, $G/V$s generated either by outward currents or from tail currents were compared (Fig. 2, B and C). Tail current $G/V$s exhibited more variance in conductance estimates, since conductance was estimated from a single point on a rapidly changing current. However, the general shape and relationship between $G/V$ curves at different pH were similar in both cases.

For descriptive purposes, single Boltzmann curves (Eq. 1) were fit to the $G/V$ curves at different pH (Fig. 2 A). The $G/V$ curves obtained at pH 7.4–8.0 were best fit with a maximal conductance that was less than that obtained at the highest pH. Increases in pH produced modest negative shifts in $V_h$ (Fig. 3 A) with little effect on $z$ (~0.4–0.5 $e$ over all pH). When $G_{max}$ was constrained to the same maximum for all $G/V$ curves, the resulting estimated shift in $V_h$ was increased, but the fit to the $G/V$ curves was poor. Thus, the shape of the $G/V$ curves over all pH suggests that, at least over the range of technically achievable command potentials, the same maximal conductance is not reached among different pH. This contrasts to the similarity in limiting conductance that is observed at different $[Ca^{2+}]$ for Slo1 channels (Cox et al., 1997). The pH-dependent differences in Slo3 conductance observed at the most positive activation potentials mirror the pH-dependent differences in single channel $P_o$ determined from single channel and variance analysis shown in the associated paper (see Zhang et al. on p. 301 of this issue).

### Regulation of Slo3 by pH May Involve Multiple pH-dependent Sites per Channel

To provide estimates of the pH dependence of the Slo3 current regulation, the conductance estimates were replotted to show the effect of pH on conductance at any potential (Fig. 3 C). Such Hill plots indicate that the pH dependence is relatively voltage independent, with half activation of conductance at any voltage occurring at $[H^+]$ concentrations of ~15–21 nM corresponding to pH values of 7.67–7.82. The Hill coefficients for such relationships ranged from 1.9 to 2.2, suggesting that multiple protonation events underlie the Slo3 current regulation. Interestingly, the apparent Hill coefficient for inhibition by proton appears to be only slightly voltage dependent, (Fig. 4 C), in contrast to the voltage dependence for activation of Slo1 by $Ca^{2+}$ or $Mg^{2+}$ (Zhang et al., 2001). Such apparent voltage dependence in the ligand effect can arise, not from voltage dependence in the binding step itself, but because of allosteric coupling of the ligand-dependent steps to the voltage-dependent closed–open equilibrium. The lack of voltage dependence in the coupling of pH and opening could reflect a weaker voltage dependence in the closed–open equilibrium.

### The Fractional Conductance of Slo3 at Negative Potentials Is Appreciable and Relatively Voltage Independent

In our typical activation protocols, we often noticed an appreciable increase in current at voltages of −100 mV or more negative as pH was increased. In the associated paper (Zhang et al., 2006), estimates of average conductance arising from putative Slo3 openings at negative potentials were made. These estimates suggested that conductance at negative potentials may be as much as 0.1% of the conductance at more positive potentials and that the voltage dependence of conductance

Published August 28, 2006

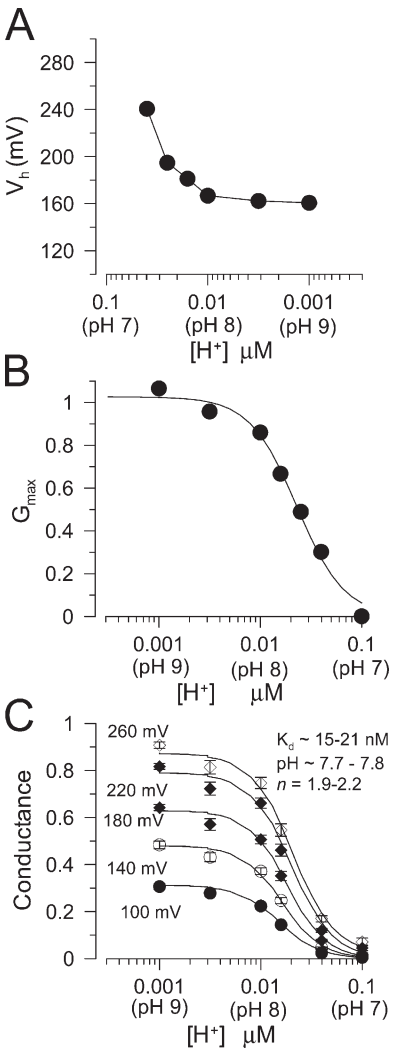


**Figure 3.** Empirical properties of Slo3 $G/V$ curves. In A, the voltage of half activation ($V_h$) is plotted as a function of proton concentration. $V_h$ estimates were based on Boltzmann fits (Eq. 1) in which $G_{max}$ was not constrained. In B, $G_{max}$ obtained from fits of Eq. 1 to $G/V$ curves at each pH are plotted as a function of $[H^+]$. The solid line is a fit of Hill equation ($G([H^+]) = G_{max}/\{1 + ([H^+]/K_d)^n\}$), yielding an effective $K_d$ of 23.3 ± 2.9 nM and with $n = 1.9 \pm 0.4$. In C, the normalized conductance is plotted as a function of $[H^+]$ for a range of command potentials. Solid lines show the best fit of a similar Hill function to conductance estimates at each voltage. The range of estimates for $K_d$ was 15–21 nM corresponding to pH of 7.7–7.8, with minimal voltage dependence in the estimates. Estimates of $n$ ranged from 1.9 to 2.2.

at negative potentials may be relatively weak. Here we attempt a macroscopic estimate of Slo3 activation at negative potentials.

To accomplish this, we examined currents at voltages from −300 mV through +300 mV in single sweeps for a limited set of pH (7.0, 7.6, and 8.5). Inspection of current traces indicates that at pH 7.0, there is little, if any, channel activation at negative potentials for the durations of steps that we have used. An example of currents from one experiment is shown in Fig. 4 for pH 7.0 and pH 8.5. A maximum of ~4 nA of current was observed in this patch at +300 mV (Fig. 4 A).

High gain examples of currents at pH 7.0, 7.6 (unpublished data), and 8.5 show that over potentials from −20 through −260 mV, there is appreciably more current at pH 7.6 and 8.5 than at pH 7.0 (Fig. 4, B and C). Over the range of −20 through −120 mV, current measured at pH 7.0 scaled linearly with voltage with no indication of any Slo3 channel openings. For the moment, making the assumption that pH does not directly affect leak conductance, the linear leak conductance determined at pH 7.0 was subtracted from currents in pH 7.6 and 8.5 to generate $G/V$ curves for each condition. This procedure resulted in log-scaled $G/V$ curves (e.g., Fig. 6 B) that approach a limiting conductance at potentials negative to −100 mV of ~0.8–1% of the maximal conductance. Of most interest, the limiting conductance appears to be relatively voltage independent over the range of −150 to −300 mV.

However, we were concerned that increasing pH may result in effects on conductance unrelated to Slo3. We have therefore examined effects of pH on currents in patches from oocytes injected with the diethylpyrocarbonate (DEPC)-buffered solutions used for cRNA injection (Fig. 4, D and E). In this case, increasing pH from 7.0 to 8.5 results in an increase in leak current, although the leak current never exhibits the flickery behavior characteristic of the Slo3 channels. For a set of four patches from DEPC-injected oocytes, estimates of leak conductance were made at pH 7.0, 7.6, and 8.5 (Fig. 6 A). Increasing pH from 7.6 to 8.5 resulted in an approximately twofold increase in a leak conductance, with no indications of any voltage dependence in the pH-dependent increase in conductance.

Because of the presence of the pH-dependent effects on leak conductance, subtraction of pH 7.0 conductances from any Slo3 currents observed at pH 8.5 will overestimate the true Slo3 conductance. We therefore employed an alternative subtraction procedure to make estimates of Slo3 conductance at negative potentials. This is illustrated in Fig. 5 A in which 10-ms traces obtained from 0 to −240 mV are shown at both pH 7.0 and pH 8.5. Although the records at pH 8.5 do not reveal a clear baseline, we have attempted to make a baseline estimate that would provide an estimate of the minimal amount of Slo3 conductance. The rationale for defining the putative baseline was based on three considerations. First, we assume that the true baseline at pH 8.5 varies linearly with voltage (Fig. 6 A), i.e., leak conductance is voltage independent. Second, we assume that some of the most positive current values in a given trace reflect excursions to the true baseline. Finally, we assume that the variance around the baseline should be similar to the variance obtained either at pH 7.0 or during steps to 0 mV. Given the rather broad shape of the current amplitude distribution, it seems

Published August 28, 2006

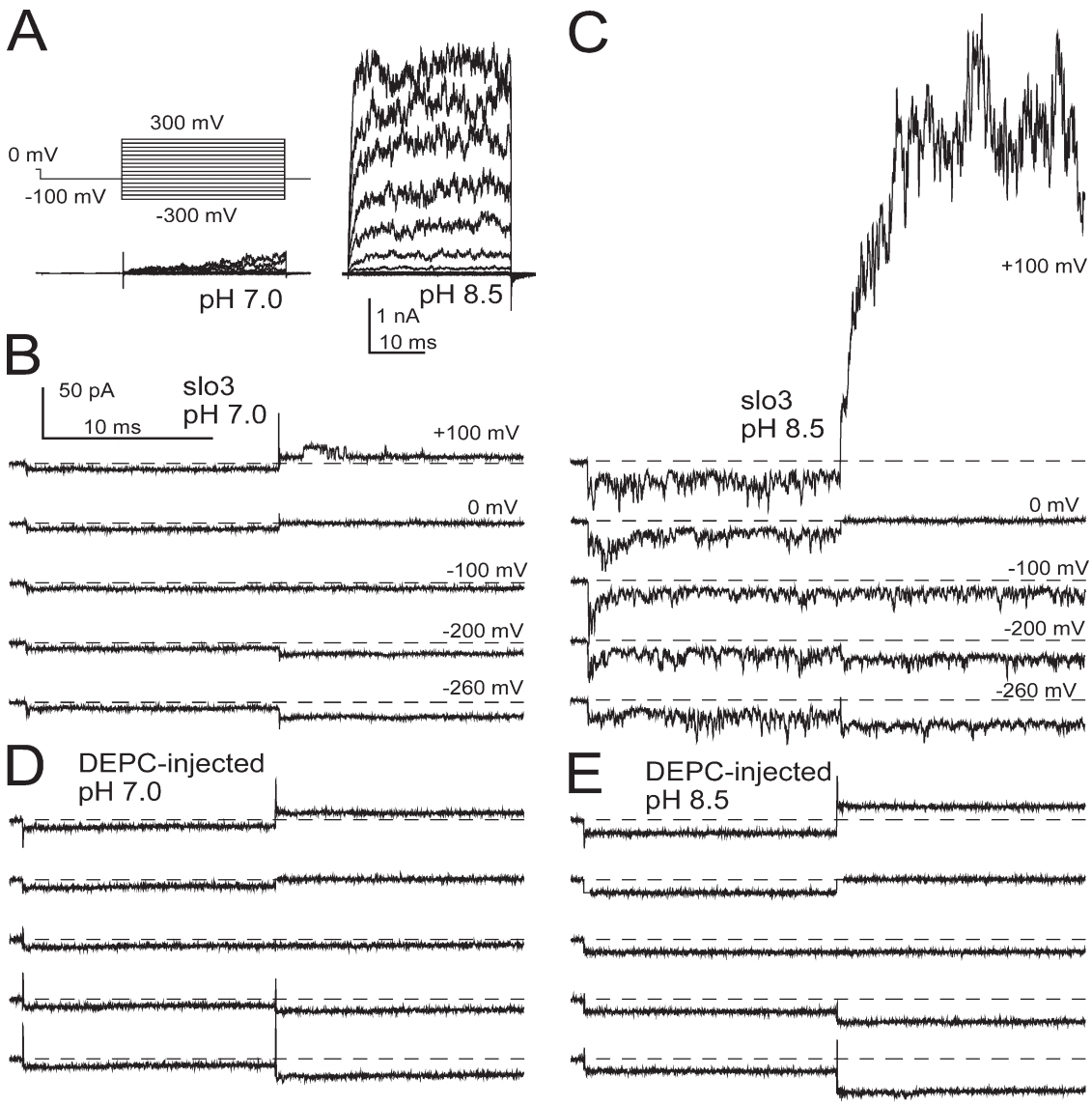


**Figure 4.** There is appreciable pH-dependent Slo3 current at negative potentials. In A, families of Slo3 currents activated by the indicated voltage protocol are shown for pH 7.0 and 8.5. Test steps to potentials from −300 to +300 mV were preceded by a conditioning step to −100 mV. Each trace corresponds to a single sweep. In B, high gain records for traces in A at negative potentials are displayed on a faster time base showing the absence of channel activity at pH 7.0. In each case, a brief period at 0 mV preceded the step to −100 mV, before the final test step. In C, similar traces at pH 8.5 show increased variance due to channel activity. In D, current traces for the same range of voltages at pH 7.0 are shown for an inside-out patch from an oocyte injected with DEPC. In E, traces are from the same patch as in D, but at pH 8.5, showing that pH increases leak current without any obvious increase in current variance.

uncertain whether any points in the distribution reflect actual baseline values. However, the purpose of this procedure is to provide a minimum estimate of the possible Slo3 current levels.

For the example in Fig. 5, the more negative dashed line on each panel indicates the baseline defined for this patch for currents at pH 8.5. This baseline estimate varies linearly with voltage, passes through the more positive current values in the trace, and, as shown in Fig. 5 B, the distribution of current values positive to this current level exhibit a range similar to the range around the baseline determined at pH 7.0. The standard deviation for single Gaussian fits to current records either at pH 7.0 or at 0 mV at pH 8.5 at 5 kHz bandwidth was ∼1.1 pA; 95% of all baseline values will be within ± 2.0 pA of the mean baseline value. For baseline estimates at pH 8.5 shown in Fig. 5, over the range of voltages from −160 through −240 mV, the baseline estimates are >2.0 pA from the most positive current values observed in the tail of the distributions. Thus, the selected baseline seems a conservative estimate of the most negative possible baseline. The mean value of all current in the record corrected for this baseline value should therefore provide a minimal estimate of Slo3

Published August 28, 2006

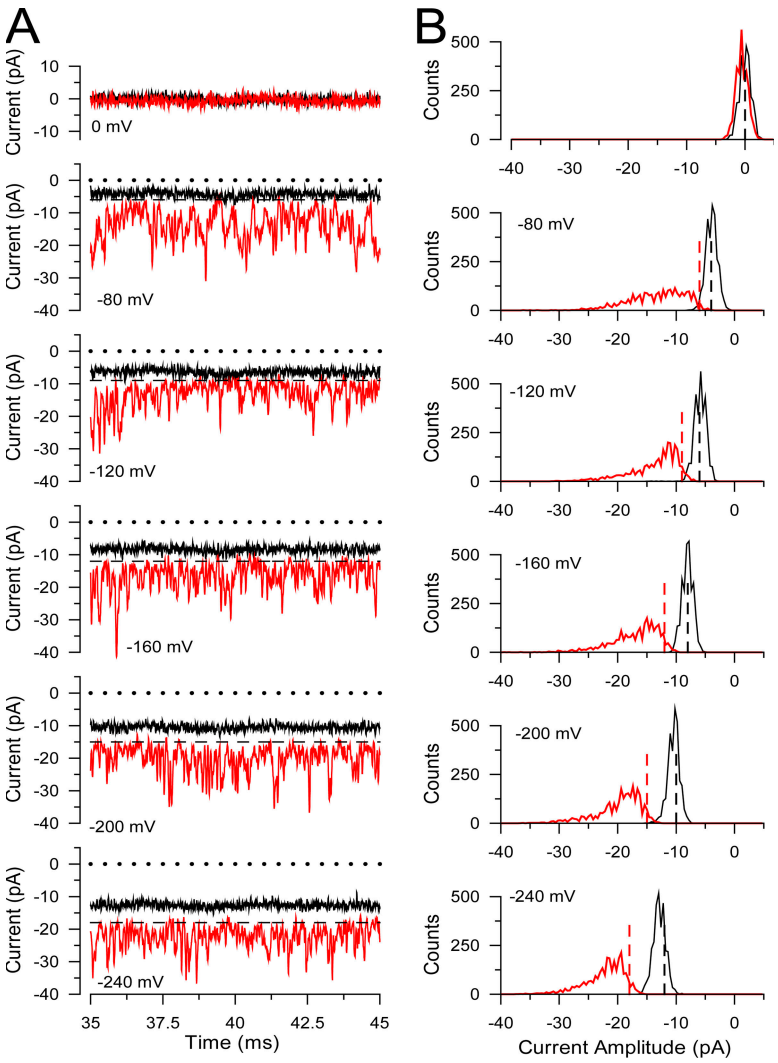


**Figure 5.** Evaluation of the average Slo3 current magnitude at negative potentials. In A, segments of currents obtained at either pH 7.0 or pH 8.5 are compared over a range of voltages for the patch shown in Fig. 4. Dotted line corresponds to the zero current level, and the dashed line corresponds to a baseline that reflects a leak conductance that is voltage independent over this range of voltages. The baseline level was chosen so that the range of current levels positive to this baseline was similar to the variance observed around the baseline for currents at pH 7.0. In B, total amplitude histograms for traces at pH 7.0 and pH 8.5 are shown, with vertical lines corresponding to the baseline used in the two cases. Note the asymmetry in the traces at pH 8.5 and symmetry at pH 7.0. The Slo3 conductance at negative potentials was estimated based on the integral of current values in the distributions at pH 8.5, after baseline subtraction.

current. However, it is likely that the true baseline will be positive to that selected (although not as positive as the pH 7.0 current level) such that the actual current arising from Slo3 will be intermediate between the two estimates. Assuming that for all patches the pH-dependent changes in leak are voltage independent (as in Fig. 5 A), the Slo3 conductances estimated by this procedure should accurately reveal the underlying voltage dependence of Slo3 activation over these potentials.

Based on this methodology, estimates of Slo3 conductance were determined and normalized to the estimates of conductance obtained in the same patches at positive potentials (Fig. 6 B). The minimum estimates of Slo3 conductance revealed a relatively voltage-independent conductance at negative potentials. An exponential fit of the conductance estimates from −300 through −220 mV yielded a limiting slope of ~0.04 *e*, while a Boltzmann fit of the values >0 mV yielded $z = 0.54 \pm 0.012$ *e*. For this same set of patches, the dependence of log(*G*) on voltage at pH 7.0, 7.6, and 8.5 is shown in Fig. 6 D, qualitatively revealing that the limiting $G_{max}$ differs at each pH.

Because of apparent reductions in single channel current amplitude observed at negative potentials in the associated paper (Zhang et al., 2006), one might raise a question regarding whether the current estimates at negative potentials can be compared with those at positive potentials. However, we established that the apparent reduction in Slo3 single channel amplitudes at negative potentials almost certainly arises from the effects of filtering and not properties of the conduction process (Zhang et al., 2006). Therefore, although filtering reduces the apparent single channel amplitude, it does not alter the net current flux passing through any individual channel over time. As a consequence, calculations of conductance based on mean current measurements at negative potentials can be normalized and compared with estimates at positive potentials.

### Allosteric Activation of Slo3 Currents

Can regulation of Slo3 by pH be described by models similar to those used to described allosteric regulation of Slo1 channels by $Ca^{2+}$? As encapsulated in Scheme 1,

Published August 28, 2006

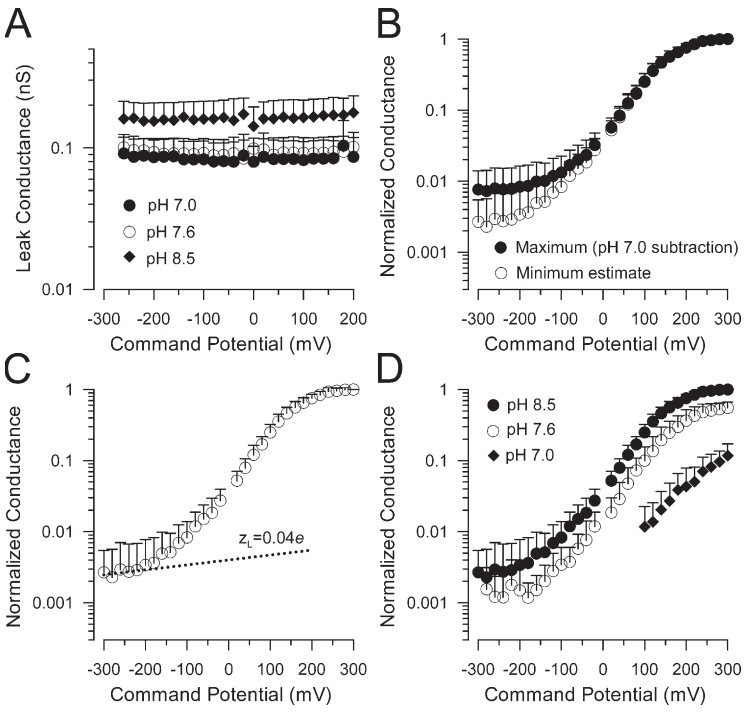


**Figure 6.** Voltage dependence of Slo3 conductance at negative potentials. In A, the voltage dependence of leak conductance in inside-out patches from DEPC-injected oocytes is displayed at each of three pH, 7.0, 7.6, and 8.5. The increase in leak conductance with increases in pH is not associated with any visually observable increase in current variance. In B, the voltage dependence of Slo3 conductance over the range of −300 to +300 mV is shown for two different methods of correction for leak current. Solid circles correspond to conductance estimates in which the leak conductance observed at pH 7.0 was subtracted on a patch by patch basis from the conductance observed at pH 8.5. This represents the maximum possible estimate of the Slo3 conductance at negative potentials. Open symbols correspond to conductance estimates derived from defining a linear leak conductance at pH 8.5 based on the most positive current over voltages from −100 through −240 mV (as illustrated in Fig. 6). This represents the minimal possible estimate of Slo3 conductance at negative potentials. In C, Slo3 conductance estimates at pH 8.5 over the range of −300 through −220 mV were fit by $G(V) = L(0)*\exp(z_L*V/kT)$, yielding an estimate of $z_L$ of 0.04 ± 0.08. After conversion of normalized conductance to absolute $P_o$ (Zhang et al., 2006), $L(0)$ was $1.25 \pm 0.10 * 10^{-3}$. In D, the $\log(G)$ vs. $V$ relationships for pH 8.5, 7.6, and 7.0 are shown.

we postulate that both voltage sensor movement and some pH-dependent process independently regulate the closed–open equilibrium. A fundamental difference between regulation of Slo1 and Slo3 is that for Slo3, interaction with the likely regulatory ion, in this case presumably protons, favors channel closure. Therefore, for Slo3, the closed Slo3 conformation corresponds to the liganded channel. As given in Scheme 1 and Eqs. 2 and 3, the formulation requires that protonation be negatively coupled to channel opening, which requires values of $C < 1$. Also, in contrast to the definition of $L$ used for Slo1 channels, in the present formulation, since $L$ defines the C–O equilibrium in the absence of protons, this represents the C–O equilibrium when the cytosolic domain is in its most activated condition.

Despite the limitations of the Slo3 $G/V$ curves and the difficulties in estimates of conductance at negative potentials both here for macroscopic currents and for unitary currents in the associated paper (Zhang et al., 2006), the available information is suitable for defining at least some of the key allosteric constants involved in Slo3 gating. It is important to keep in mind that interpretation of the present macroscopic measurements depends critically on the fact that in the associated paper (Zhang et al., 2006) we have demonstrated that Slo3 single channel conductance varies ohmically with voltage and is independent of pH. This provides assurance that any pH-dependent effects on macroscopic currents do arise from regulation of the conformational equilibrium rather than from direct effects on ion conductance. Using the estimates of the voltage and pH dependence from the unitary current measurements to renormalize the macroscopic conductance estimates, Fig. 7 displays the macroscopic $\log(G)/V$ curves in terms of effective $P_o$.

### Estimation of $z_L$, $L(0)$, $D$, and $z_J$

At very negative potentials, Slo1 voltage sensors almost exclusively reside in resting positions (Horrigan and Aldrich, 2002). Hence, at sufficiently negative potentials, changes in conductance and the voltage dependence of conductance reflect primarily the C–O equilibrium and its coupling to the ligand-dependent equilibrium. Although direct measurements of the Slo3 voltage sensor equilibrium are not available, the Slo3 $\log(G)$ vs. $V$ curve exhibits two regions of distinct slopes, similar to Slo1, characteristic of the $L$ and $J$ equilibria. Thus, at the most negative potentials, the residual voltage dependence of activation should reflect the intrinsic voltage dependence of $L$. The voltage dependence of conductance under conditions where voltage sensors are largely inactive is described by the following scheme.

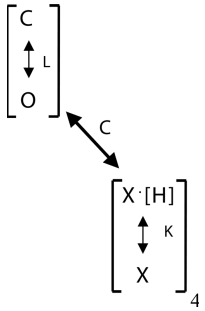


(Scheme 2)

Published August 28, 2006

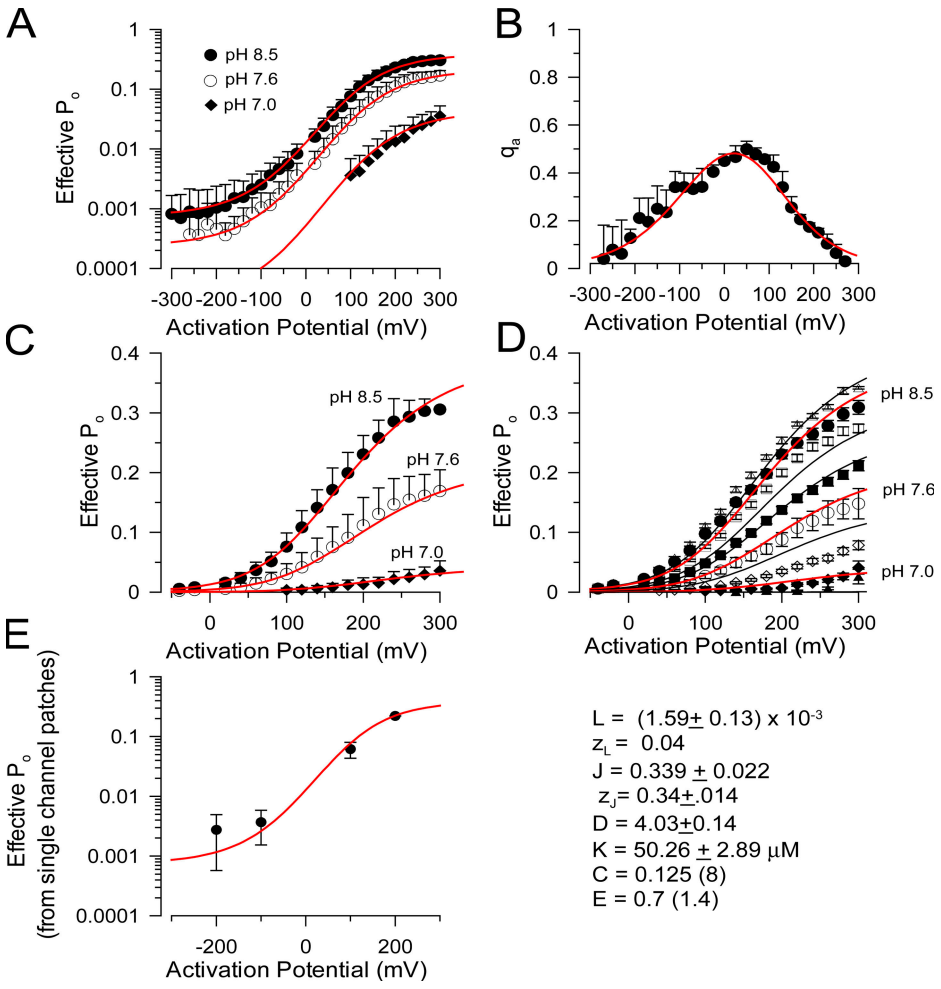


**Figure 7.** Slo3 steady-state conductance can be described by Scheme 1. In A, the $\log(P_o)$ vs. voltage relationships at pH 7.0, 7.6, and 8.5 were fit (red line) with Scheme 1, assuming $z_L = 0.04$, and constraining $C$ and $E$. Macroscopic conductances were converted to $P_o$ based on the estimates of unitary current $P_o$ in the accompanying paper (Zhang et al., 2006). In B, $q_a$, the mean activation charge displacement, was determined from the slope of the $\log(P_o)$ vs. $V$ relationship. Each $q_a$ estimate was determined from the slope of the $\log(P_o)$ vs. $V$ values for each sequential set of four voltages, covering a 60-mV range. Error bars correspond to the confidence limit on the fit to the slopes. The red line corresponds to the expected $q_a/V$ relationship based on the fit shown in A. In C, the data in A were replotted on a linear scale to show the adequacy of the fit at higher $P_o$ values. In D, the predictions of the allosteric derived from the fit shown in A are compared with the $P_o$ vs. $V$ relationship shown in Fig. 2 for a different set of patches in which currents were measured over a wider range of pH. Red lines correspond to pH 7.0, 7.6, and pH 8.5, respectively, with solid symbols reflecting those concentrations. In E, estimates of the voltage dependence of single channel $P_o$ provided in the accompanying paper (Zhang et al., 2006) show good agreement with the expectations derived from fitting A.

Based on Scheme 2, Eq. 3 (Horrigan and Aldrich, 2002) reduces to

$$P(V,[H]) = \frac{1}{1+\frac{1}{L(0)e^{z_L V/kT}}\left[\frac{(1+K)}{(1+KC)}\right]^4}. \quad (4)$$

Since, at negative potentials and over all pH, the normalized fractional conductance is $<0.01$, $(1 + K)^4 >> L(1 + KC)^4$. Eq. 4 can then be simplified to

$$P(V) = L\left(\frac{1+KC}{1+K}\right)^4. \quad (5)$$

Furthermore, at the most elevated pH, $(1 + KC)/(1 + K) \sim 1$ such that

$$P(V) = L(0)\exp\left(\frac{z_L FV}{RT}\right). \quad (6)$$

Therefore, the relationship between conductance and voltage at negative potentials and elevated pH allows definition both of $L(0)$ and $z_L$, where $L(0)$ for Slo3 is defined as the closed–open equilibrium with an unliganded cytosolic structure.

The fit of the limiting conductance at negative potentials for Slo3 yielded an estimate of $z_L = 0.04$ $e$. This value corresponds reasonably well with the estimate of voltage dependence of single channel conductance of 0.075 $e$ over the more positive voltage range of −100 to −200 mV (Zhang et al., 2006). In accordance with the definition of $L$, $L(0)$ therefore corresponds to the Y intercept of the limiting conductance observed at negative potentials. After conversion of the normalized conductance (Fig. 6 C) to absolute $P_o$ (Fig. 7 A) as determined in the associated paper (Zhang et al., 2006), $L(0)$ at pH 8.5 was $(1.25 \pm 1.0) * 10^{-3}$. Since at pH 8.5, Slo3 activation is somewhat less than maximal, we would expect the true value for $L(0)$ to be somewhat higher.

Finally, the $\log(G)$ vs. $V$ relationship provides some information about $D$, the coupling factor between voltage sensor movement and channel opening and also $z_J$,

Published August 28, 2006

the voltage dependence of the voltage sensor equilibrium. At elevated pH, channel $P_o$ is given by

$$P(V) = \frac{1}{1 + \frac{1}{L}\left[\frac{1+J}{(1+JD)}\right]^4}. \quad (7)$$

For the case that $L$ has a negligible voltage dependence (i.e., $z_L$ is small) and that the most positive potentials strongly favor voltage sensors in activated states, the ratio between $P_o$ at the most positive and negative potentials is approximated by

$$P(V_{\max})/P(V_{\min}) = \left(\frac{1 + DJ(0)e^{z_J V_{\max}/kT}}{1 + J(0)e^{z_J V_{\max}/kT}}\right)^4 \sim D^4. \quad (8)$$

For Slo3 at pH 8.5, a change in voltage from −300 to +300 results in an ∼250–400-fold increase in channel open probability. This suggests a value for $D$ of ∼4–4.5.

Based on the $\log(P_o)/V$ relationship, the above considerations place important constraints on several of the allosteric factors required to describe Slo3 gating equilibrium. It would also be desirable to define parameters for the protonation equilibrium under limiting conditions, e.g., with voltage sensors either in resting or active conditions. Although the available $G/V$ curves essentially define the foot of the concentration–response curve for the effects of protonation, the absence of a measurable current at low pH means that estimates of the coupling constant between the protonation equilibrium and $L$ will be imprecise.

Using the above considerations to constrain some of the parameters, we used Eq. 2 to fit the $\log(P_o)/V$ relationship. $z_L$ was constrained to 0.04 *e*. $C$ was constrained to 0.125, which is the inverse of the constant coupling $Ca^{2+}$ binding to $L$ in Slo1 (Horrigan and Aldrich, 2002); $E$ was fixed at 0.7 (corresponding to a value of 1.4 for Slo1). With these constraints, an iterative fitting procedure rapidly converged (Table I) and the resulting values for $L(0)$ ($[1.59 \pm 0.13] * 10^{-3}$) and $D$ ($4.03 \pm 0.14$) were in reasonable correspondence with the expected values based on the $\log(P_o)$ vs. $V$ relationship given above. If $C$ was allowed to vary, iterative fitting did not reach a convergence as $C$ drifted toward 0. Changes in $C$ to values other than 0.125 did not improve the ability of the model to approximate the unique characteristics of the Slo3 datasets. Similarly, allowing $E$ to vary did not result in any improvement in the fits and suggests that effects of pH on the voltage-sensing apparatus itself are unlikely to underlie the pH-mediated effects on Slo3 gating. Somewhat improved fits were obtained if $z_L$ was allowed to vary with the optimal fits occurring as $z_L$ approaches 0. $z_J$ for Slo3 is somewhat smaller than for Slo1, 0.34 vs. 0.58, and this appears consistent with the shallower macroscopic $G/V$ curves observed for Slo3.

TABLE I

*Allosteric Constants Comparing Slo3 and Slo3 Activation*

| Parameter | Slo3 | Slo1 Horrigan/Aldrich | Slo3 with $z_L \rightarrow 0$ |
|---|---|---|---|
| $L$ | $(1.59 \pm 0.13) * 10^{-3}$ | $9.8 * 10^{-7}$ | $(0.97 \pm 0.007) * 10^{-3}$ |
| $z_L$ *e* | 0.04[a] | 0.3 | 0.002[a] |
| $J_0$ | 0.34 ± 0.02 | 0.03 | 0.32 ± 0.02 |
| $z_J$ *e* | 0.34 ± 0.014 | 0.58 | 0.31 ± 0.01 |
| $D$ | 4.03 ± 0.14 | 25 | 5.18 ± 0.17 |
| $K$ (μM) | 50.26 ± 2.89 | 11 | 51.4 ± 2.6 |
| $C$ | 0.125[a] (8) | 8 | 0.125[a] (8) |
| $E$ | 0.7[a] (1.4) | 2.4 | 0.7[a] |
| $V_{hc}(J)$ mV | 80.1 | 152.7 | 92.8 |
| SSQ | 0.639 | | 0.513 |

Note that, for both Slo1 and Slo3, $L(0)$ is defined as closed open equilibrium in the absence of the modulating ligand, i.e., $Ca^{2+}$ and $H^+$, respectively. $V_{HC}(J)$ was calculated from $(kT*\ln(J_0)/z_J)$. No convergence occurred when $C$ is unconstrained; $C$ drifts to 0. Fits are improved with $z_L$ approaching 0.

[a]Value constrained during fitting procedure.

Another indication of the voltage dependence of charge movement can be provided by determination of the mean activation charge displacement, $q_a$ (Sigg and Bezanilla, 1997). $q_a$ is calculated from the logarithmic slope of the $P_o/V$ relationship, and values of $q_a$ at negative potentials provide a direct estimate of the limiting $z_L$ value (Ma et al., 2006). The $q_a/V$ relationship for Slo3 is given in Fig. 7 B, along with the expected $q_a/V$ relationship based on the fit to the $\log(P_o)/V$ relationship. The ability of the set of parameters defined by fitting the $\log(P_o)/V$ relationship to describe other aspects of our Slo3 results is also summarized in Fig. 7 (C–E). In C, a plot of $P_o/V$ for the data in A shows the adequacy of the fitted curves at the more positive activation potentials. For data shown earlier in Fig. 2 from a different set of patches over a wider range of pH, the same parameters also provide a reasonable description of the change in conductance both as a function of voltage and pH (Fig. 7 D). Finally, the same set of parameters describes the $P_o/V$ relationship (Fig. 7 E) based on the single channel analysis presented in the associated paper (Zhang et al., 2006).

Values for all parameters are given in Table I. Visually, the parameters predict $G/V$ curves that capture well the general behavior of the experimentally obtained $G/V$ curves, although at lower pH, the shifts in $G/V$ curves are less well described. It is possible that secondary effects of lower pH may also influence the $G/V$ curves. For example, an activating effect of pH below 7.0 has been observed in Slo1 (Avdonin et al., 2003). However, a number of conclusions are clear. First, the general allosteric model given in Scheme 1 is a reasonable model for Slo3 activation, suggesting that both a protonation-dependent process and voltage sensor movement independently couple to the Slo3 closed–open conformational change.

Published August 28, 2006

Second, the two major factors that contribute to the differences in $G/V$ curves between Slo1 and Slo3 are, first, that for Slo3, the intrinsic voltage dependence of the C–O equilibrium, defined by $z_L$, is much weaker and, second, that coupling of voltage sensor movement to channel opening, defined by $D$, is weaker.

To illustrate these differences and the impact of changes in $z_L$ and $D$, versus changing other parameters, the parameters given in Table I were used to generate the expected $\log(P_o)$ vs. $V$ relationship for pH 7.0, 7.6, and 8.5 (Fig. 8 A) and compared with similar predictions for Slo1 based on parameters from Horrigan and Aldrich (2002) also given in Table I. Then, the parameters $z_L$ and $D$ were changed individually ($D$, Fig. 8, C and D; $z_L$, Fig. 8, E and F) or together (Fig. 8, G and H) to illustrate that these two parameters can account for most of the major differences in behavior between Slo1 and Slo3 $G/V$ curves. Changes in other parameters, $L(0)$, $J(0)$, or $C$, produce changes that do not account for the differences between Slo1 and Slo3, while the difference in $z_J$ between Slo1 and Slo3 contributes in part to the shallower $G/V$ relation for Slo3.

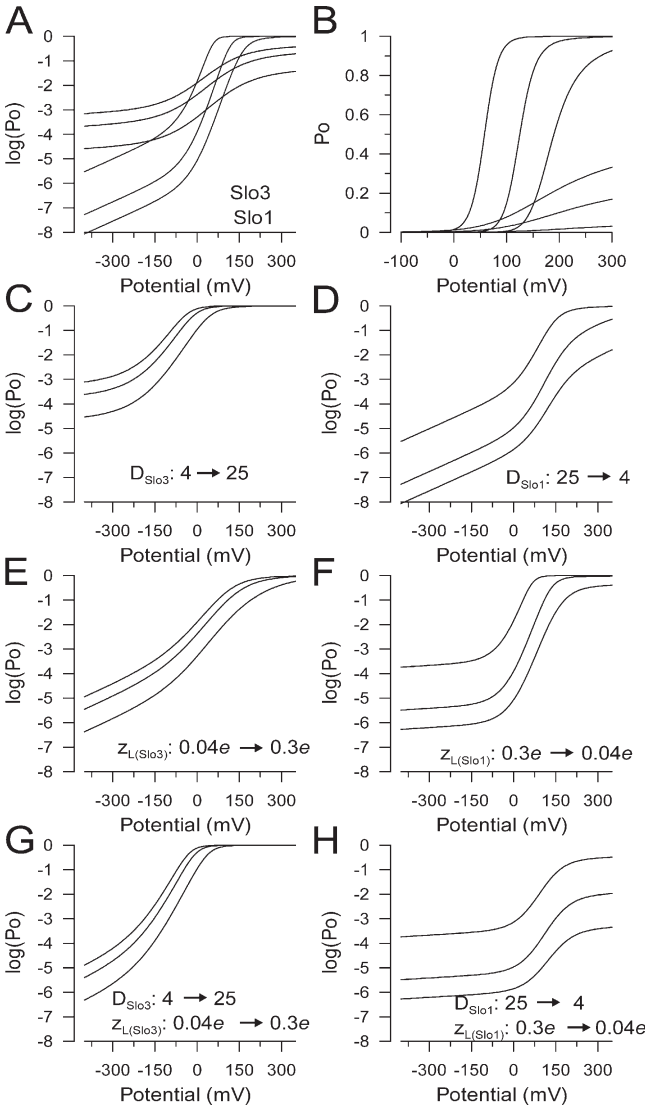


**Figure 8.** The primary differences between the voltage dependence of Slo3 and Slo1 conductance arise from differences in $z_L$ and $D$. In A, predicted $\log(P_o/V)$ relationships for Slo3 based in parameters in Table I for pH 7.0, 7.6, and 8.5 are shown in red, along with predictions for Slo1 based on values from Horrigan and Aldrich (2002; and Table I) for $[Ca^{2+}]$ of 0.01, 1, and 10 μM. In B, the same relationships are plotted on a linear $P_o$ scale. In C, the value of $D$ for Slo3 was changed from 4 to 25 to approximate that for Slo1, resulting in a similar maximal saturating $P_o$ at each pH. In D, the value of $D$ for Slo1 was changed from 25 to 4. In E, $z_L$ for Slo3 was changed from 0.04 $e$ to 0.3 $e$ to approximate that for Slo1, changing both the limiting slope at negative potentials and the tendency toward saturation at positive potentials. In F, the value of $z_L$ for Slo1 was changed to 0.04 $e$. In G, values for $z_L$ and $D$ for Slo3 were simultaneously changed to those describing Slo1, while in H, values for $z_L$ and $D$ for Slo1 were changed to those characteristic of Slo3. In both cases, simultaneously changing both $z_L$ and $D$ in large measure accounts for the characteristic differences between Slo1 and Slo3.

## Slo3 Activation and Deactivation Kinetics Exhibit Two Exponential Components

We now provide a description of the activation and deactivation behavior of Slo3 gating kinetics.

*Current Activation.* Fig. 9 illustrates the time course of Slo3 current activation and its dependence on pH and depolarization. Traces plotted on a linear time base (left column) are fit with single exponential functions, while middle and righthand columns compare the ability of single or double exponential functions to describe the activation behavior. At both lower (7.4) and higher pH (9.0), activation is reasonably well described by a single exponential function over the full range of activation voltages (Figs. 9 and 10). However, over the range of pH (7.6–8.5) that produces the primary shifts in G/V curves, two exponential components are clearly required.

The two exponential components in the activation time course of Slo3 contrast markedly with the behavior of Slo1 (Zhang et al., 2001; Horrigan and Aldrich, 2002). Despite the complexity in Slo1 gating models involving both $Ca^{2+}$- and voltage-dependent transitions, for Slo1 it is thought that voltage sensor movement and $Ca^{2+}$ binding steps are rapid and essentially in equilibrium during the time course of current activation. Thus, the observed kinetic relaxation is thought to reflect the conformational change corresponding to opening of the channel (Zhang et al., 2001; Horrigan and Aldrich, 2002).

To assess qualitatively the contributions of pH- and voltage-dependent processes to the activation time course, currents activated under different conditions were normalized and the activation time courses compared either as a function of voltage (Fig. 10 A) or of pH (Fig. 10 B). For patches with smaller currents and

Published August 28, 2006

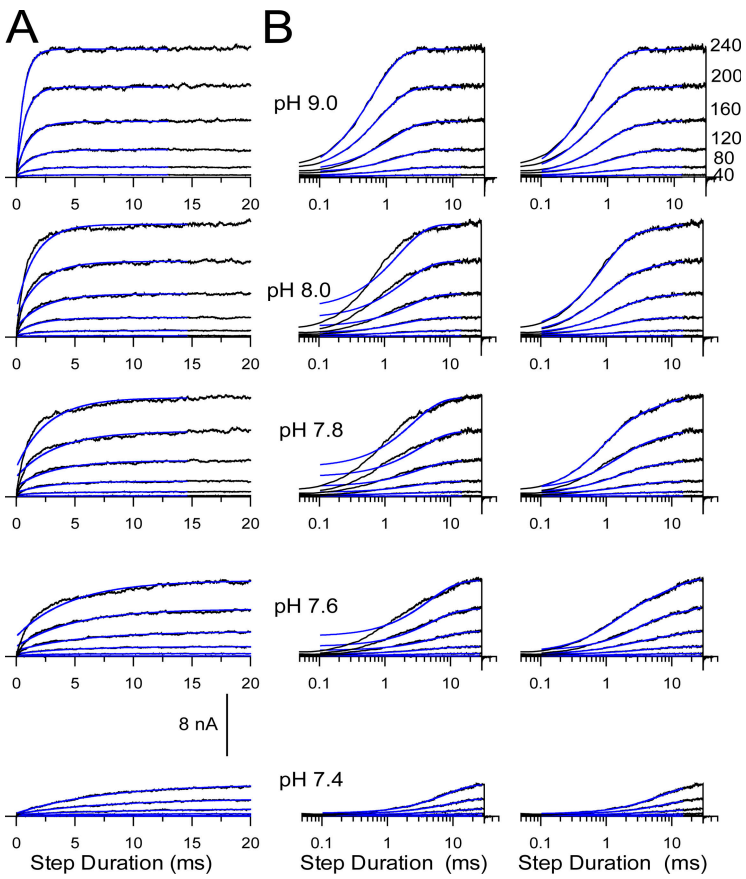


**Figure 9.** Slo3 activation time course is defined by two exponential components. In A, the Slo3 activation time course is illustrated for pH from 9.0 to 7.4 (top to bottom) at voltages from +40 to +240 mV. Blue lines indicate single exponential fits ($I(t) = A\exp(-t/\tau) + C$) to the activation time course, which at pH 7.6, 7.8, and 8.0 fails to describe the activation time course. In B, the same traces are shown on a logarithmic time axes along with either a single exponential (left traces) or a two exponential ($I(t) = A_s\exp(-t/\tau_s) + A_f\exp(-t/\tau_f) + C$; right traces) fit to the activation time course. The activation time course is best described by two exponential components.

at lower pH, stochastic fluctuations in currents contributed to variability in estimates of fast and slow time constants and the relative amplitude of each component. However, the overall trends of the behavior of each component were consistent among all patches. An 80-mV change in activation potential produces an ~1.5–2-fold change in the half-current activation time irrespective of the pH (Fig. 10 A). In contrast, the time of half activation of current shifts approximately an order of magnitude as pH is increased from 7.4 to 9.0, irrespective of the activation voltage (Fig. 10 B). Qualitatively, this behavior is not unlike that of Slo1. For Slo1, increases in $Ca^{2+}$ from 1 to 100 μM produce an ~10-fold change in activation time constant at a given potential, while an 80-mV change in activation voltage produces an approximately twofold change in activation time constant (Zhang et al., 2001). Thus, despite the differences in the number of exponential components required to describe the activation time course, qualitatively the general effects of ligand and voltage on overall rates of activation seem similar between Slo1 and Slo3.

Examination of the specific changes in the fast ($\tau_f$) and slow ($\tau_s$) components as a function of changes in voltage reveals that over the range of voltages from 120 to 240 mV, there is an ~1.5-fold decrease in $\tau_f$, with little clear change in $\tau_s$ (Fig. 11 A). Similarly, changes in pH are associated with rather negligible changes in either $\tau_f$ or $\tau_s$. In general, $\tau_s \sim 10$ ms, while $\tau_f \sim 1$ ms, and at pH 7.4, the single exponential describing the activation time course appears to be predominantly $\tau_s$, while at pH 9.0, the single exponential appears to be exclusively $\tau_f$. At intermediate pH, despite the small changes in the actual values of $\tau_s$ and $\tau_f$, there is a prominent pH-dependent change in the relative amplitudes of the two time constants (Fig. 11 B). Whereas at pH 8.0, the fast relaxation contributes ~75% to the total activation time course, at pH 7.6, the fast relaxation contributes only ~40%. Thus, there is a steep dependence on pH of the ratio of the amplitudes of the two components, $A_s/A_f$, with small effects on the actual time constants themselves. Voltage, per se, has minimal effect on the relative contributions of the two components over the range of +120 to +240 mV (Fig. 11 B). Thus, the differences in the relative effects of pH and voltage on the amplitude ratios account for the stronger effect of pH than voltage on overall activation rate.

We next evaluated the contribution of the slow and fast current components to the overall absolute conductance. Fitted estimates of the slow and fast amplitude components were converted to conductances and then normalized to the overall maximum conductance observed in a given patch at pH 9.0. For the slow component (Fig. 11 D), given that pH 7.0 activates very little current, the absolute magnitude of this slow conductance

Published August 28, 2006

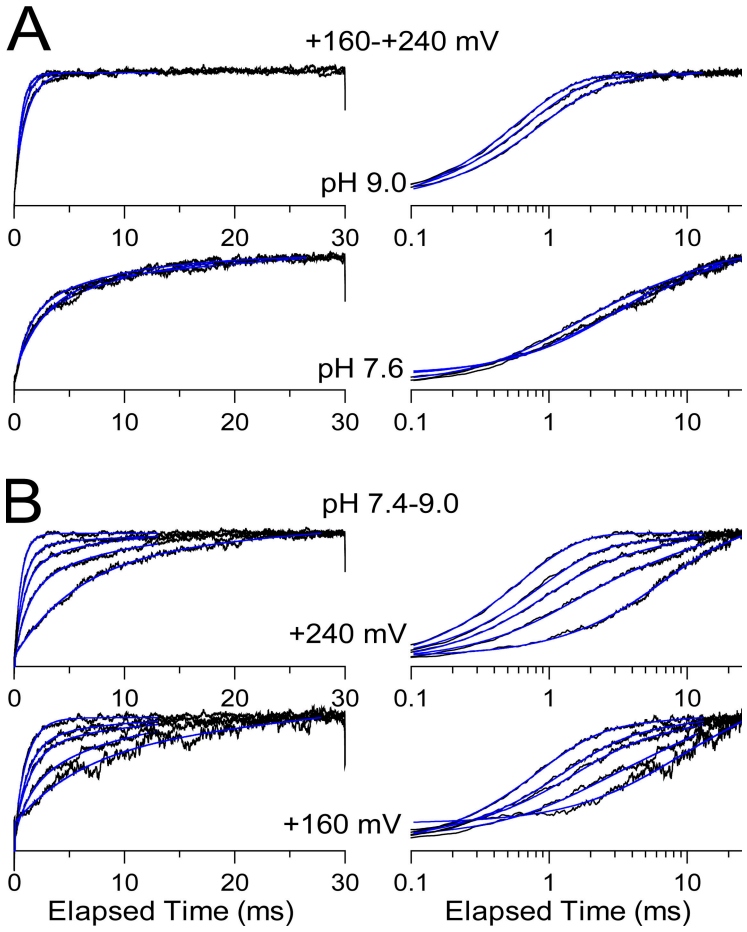


**Figure 10.** Changes in Slo3 activation time course is more strongly influenced by pH than voltage. Traces from Fig. 9 were normalized and grouped to illustrate the dependence of activation time course either on voltage (A) or pH (B). In A, traces on the top show the activation time course at pH 9.0 for +160, +200, and +240 mV on either a linear (left) or logarithmic time base. Blue lines correspond to a fit of two component exponential function. Traces in the bottom panels of A show the corresponding activation time course for pH 7.6 for +160, +200, and +240 mV. In B, the activation time course for normalized currents is compared as in A but for pH 7.4, 7.6, 7.8, 8.0, and 9.0 at +240 mV (top sets of traces) and at +160 mV (bottom sets of traces). Blue lines are two component exponential fits.

increases from pH 7.0 through pH 7.6, but then decreases at higher pH. Because of its small amplitude, no estimate of the magnitude of the slow component of conductance was made above pH 8.0. In contrast, the fast component increases over all pH (Fig. 11 E) and the sum of the amplitudes of the two current components estimated from fitting the activation time course agrees closely with direct measurements of the steady-state conductance (Fig. 11 F). Thus, the changes in the ratio of the fast and slow component with increases in pH involve both an increase in the absolute contribution of the fast component and a decrease in absolute magnitude of the slower component.

*Deactivation of Slo3 macroscopic currents.* Another unusual feature of the Slo3 current is the small amplitude and rapid time course of the tail current after repolarization to negative potentials. To examine this more closely, mSlo3 current was activated by depolarizations to +200 mV, followed by repolarizations to potentials between −200 and +180 mV at pH from 7.4 to 9.0 (Fig. 12). At potentials negative to 0 mV, with a typical recording bandwidth of 10 kHz, two exponential components were clearly observed in the tail current (Fig. 12 B; Fig. 13) with the more rapid component having a time constant of <50 μs. Empirically, the rapid deactivation of Slo3 tail current results in an apparent inward current rectification in the instantaneous current–voltage curve. We tested whether the rapid deactivation might be influenced by particular components of our extracellular solution. In addition to $K^+$, our usual extracellular solutions contained 10 mM HEPES and also 2 mM $Mg^{2+}$. Extracellular solutions containing either 1 mM HEPES or 1 mM EDTA and no added $Mg^{2+}$ had no effect on the tail currents (unpublished data).

The general properties of the two components of deactivation are summarized in Fig. 13. Tail currents at different voltages (Fig. 13, A–C) and pH (Fig. 13, D–F) were compared on both linear and logarithmic time scales. Fits of a two component exponential are required to describe the current decays. For changes in tail current potential (Fig. 13, A–C), the primary change in the tail currents is a decrease in the relative amplitude of the slow component ($\tau_s$) of tail current at more negative potentials (Fig. 13 C). For changes in pH at a fixed voltage, the properties of the tail currents are remarkably similar (Fig. 13 F). Examination of the dependence of the two components on voltage and pH reveals some interesting features. First, at a given pH, voltages from −40 through −200 have little effect on $\tau_s$, and only

Published August 28, 2006

weak effects on $\tau_f$ (Fig. 13 G), although the contribution of the fast component increases at more negative voltages (Fig. 13 H). Second, at −200 mV, changes in pH from 7.4 to 9.0 have essentially no effect on $\tau_f$ or $\tau_s$ or the ratio between the two components, despite the fact that the outward current varies by at least twofold at the activation potential of +200 mV.

Because both activation and deactivation time course exhibit two exponential components, it is tempting to assume that each component describing the activation time course correlates with one of the two components contributing to deactivation. However, the fast component of deactivation may not be directly related to either of the components seen in the activation time course. Specifically, the fast time constant of current activation and the slow time constant of deactivation have very comparable values and both only exhibit a weak voltage dependence, if any. This suggests that the activation $\tau_f$ and deactivation $\tau_s$ may reflect the same underlying process. In contrast, for the fast component of deactivation, there is no obvious correspondence to any measured component of the activation process. Perhaps related to the idea that the fast component of tail current may be unrelated to either of the reported time constants of current activation, the flickery Slo3 single channel behavior (Zhang et al., 2006) suggests there is a fast component of Slo3 gating that is not rate limiting for the macroscopic activation time course.

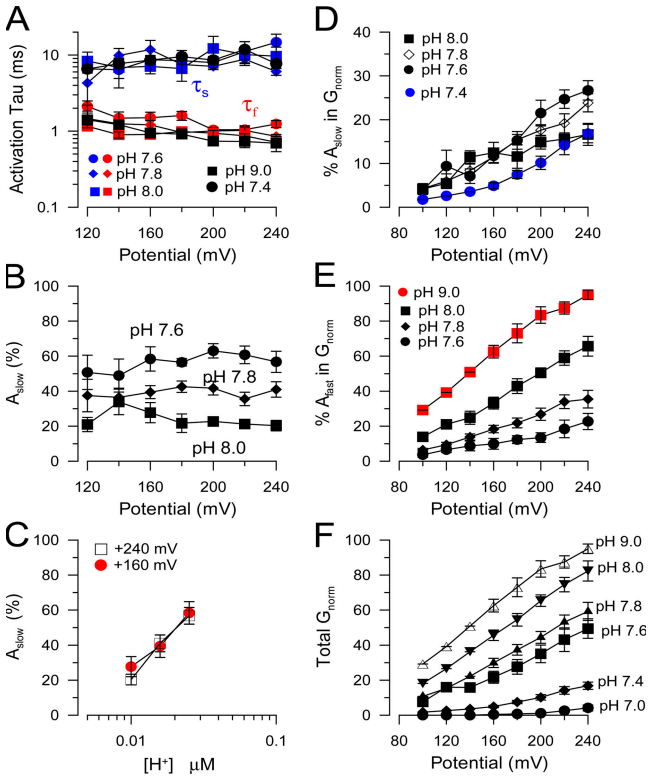


**Figure 11.** Properties of two components of slo3 activation. In A, fast (red) and slow (blue) time constants of activation at the indicated pH are plotted as a function of activation potential. Error bars are SEM of seven to eight estimates. The single exponential described activation at pH 9.0 closely approximates the fast time constant of activation, while the single exponential describing activation at pH 7.4 approximates the slow time constant. The fast time constant appears to become somewhat faster with depolarization. In B, the percent of the slow activation component is plotted as a function of voltage for three different pH. The relative contribution of the slow component does not change with command potential, but decreases with increases in pH. In C, the percent of the slow component is plotted as a function of pH for two different voltages. The percent of the slow component increases as pH is decreased. At pH 7.4, slow component contribution approaches 100%, while at pH 9.0, it is less than 5%. In D, the absolute contribution of the slow component to normalized conductance is plotted as a function of voltage for different pH. In E, the contribution of the fast component to conductance is plotted as a function of voltage for different pH. All conductance values in D and E were normalized within patches to the maximum conductance observed at pH 9.0. In F, the voltage dependence of the sum of the fast and slow component of conductance is illustrated, approximating the macroscopic steady-state *G/V*s.

## DISCUSSION

Slo3 exhibits substantial amino acid homology with its $Ca^{2+}$-dependent relative, Slo1 (Schreiber et al., 1998); in fact, the overall homology between mSlo1 and mSlo3 slightly exceeds that between the functional homologues, mSlo1 and dSlo1 (Butler et al., 1993). Despite these homologies, Slo1 and Slo3 differ in a number of fundamental ways, including the nature of the ligand-dependent regulation, basic aspects of single channel conductance, and perhaps even ion selectivity (Schreiber et al., 1998). The marked sequence similarities between the two channels has made them useful for chimeric studies of channel function (Schreiber et al., 1999; Moss and Magleby, 2001; Shi et al., 2002; Xia et al., 2004), and such a strategy may prove useful in elucidating the fundamental similarities and differences in the underlying machinery by which gating in both channels is regulated. The results presented in this and the associated paper (Zhang et al., 2006) provide the basic empirical description of Slo3 properties necessary to begin examination of the underlying mechanistic differences between Slo1 and Slo3.

The key differences between Slo3 and Slo1 are the following. First, Slo3 exhibits an apparent pH-dependent limiting conductance at +300 mV, in contrast to the relatively similar maximal conductance observed among different $Ca^{2+}$ in Slo1. Second, voltage dependence of conductance at negative potentials is weaker for Slo3 than for Slo1. Third, the estimates of maximal channel $P_o$ under conditions of strong activation are <0.4 compared with values for Slo1 that are >0.9 (Zhang et al., 2006). Fourth, there are multiple components in the activation and deactivation kinetics for Slo3 that differ from the largely single exponential time course of Slo1 relaxations. Finally, in contrast to the relatively stable

Published August 28, 2006

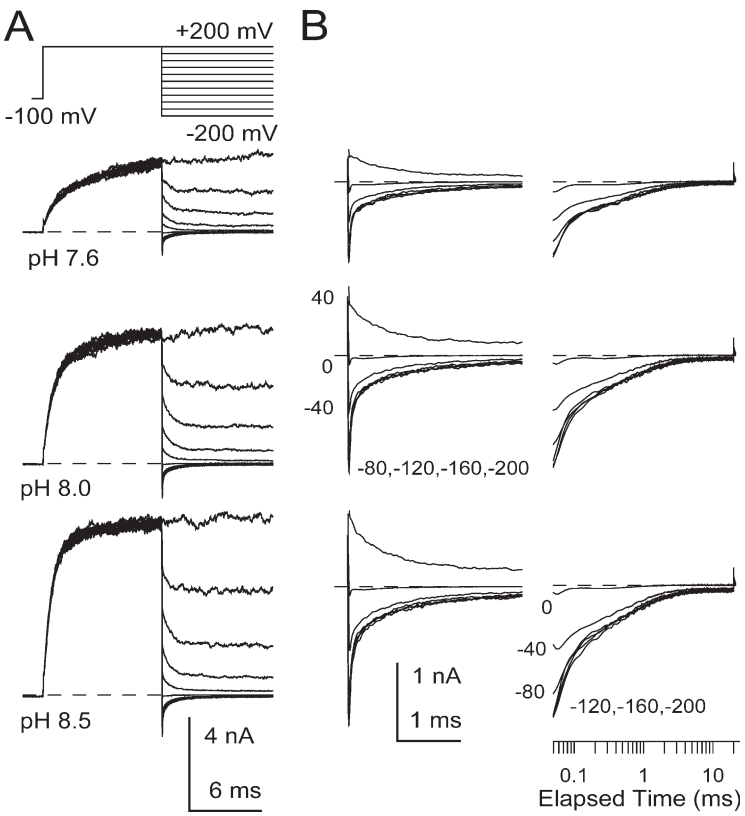


**Figure 12.** Slo3 deactivation contains two components. In A, the indicated voltage step protocol was used to examine tail current properties at potentials from −200 to +180 at various pH as indicated. Peak tail current at −200 mV is markedly nonohmic in comparison to current at +200 mV. 50 kHz sampling rate; 10 kHz filter. In B, the tail currents in A at potentials from +40 to −200 mV shown on a faster time base to emphasize the fast and slow components of the decay process. Traces on the left are shown on linear time scale, while those on the right are plotted on a logarithmic time scale.

open current levels of Slo1 single channels, Slo3 single channels exhibit a rapid opening and closing that prevents simple definition of a unitary current level (Zhang et al., 2006). We now address the significance of these differences in terms of the underlying allosteric mechanism of channel gating.

### Allosteric Regulation of Slo3 Channels: Similarities and Differences with Slo1

We have previously shown that the pH dependence of Slo3 is conferred by the C-terminal cytosolic module of Slo3 and does not arise from the Slo3 pore domain (Xia et al., 2004). Furthermore, this earlier work and the analysis of the effects of pH on single Slo3 channels (Zhang et al., 2006) indicate that the changes in $G/V$ curves produced by pH do not result from inhibition of the pore by pH. These factors have allowed us to use macroscopic conductance measurements under different conditions to test the suitability of the general HA allosteric model (Horrigan and Aldrich, 2002) to account for the regulation of Slo3 conductance by pH. To apply this model to Slo3, we have postulated that binding of a proton is negatively coupled either to $L$ or $J$, the constants for the central closed–open equilibrium and the voltage sensor equilibrium, respectively. This assumption may seem surprising given that for Slo1 binding of the cation $Ca^{2+}$ is positively coupled to the central closed–open equilibrium, and we will give this point additional consideration below. For the moment, let us first consider to what extent the present results support the idea that a similar allosteric model may apply to both Slo1 and Slo3.

For the general allosteric model in Scheme 1, macroscopic Slo3 $G/V$ curves are insufficient to define the full set of parameters given in Eq. 3. For Slo1, the work of Horrigan and Aldrich (2002) used a number of limiting conditions that allowed independent definition of a number of the key parameters required to describe Slo1 regulation. Here, several factors precluded independent definition of all necessary parameters for Slo3. In particular, a limiting conductance could not be defined at the lowest pH, thus precluding precise definition of C, in particular. Furthermore, at present we do not have direct information derived from gating current measurements regarding the voltage sensor equilibrium. Finally, given the very brief Slo3 openings observed at negative potentials, a number of assumptions were made to allow analysis of the Slo3 currents observed at negative potentials both here and in the associated paper (Zhang et al., 2006).

Yet, despite these limitations, the estimates of Slo3 allosteric parameters obtained here very adequately describe Slo3 behavior within the context of Scheme 1. The two parameters that appear to account for most of the differences in shape of $G$-$V$ relations between Slo3 and Slo1 were the intrinsic voltage dependence ($z_L$: 0.3 for Slo1 and ∼0.04 for Slo3) of $L$, and the strength of coupling ($D$: 25 for Slo1 and 4 for Slo3) between voltage

Published August 28, 2006

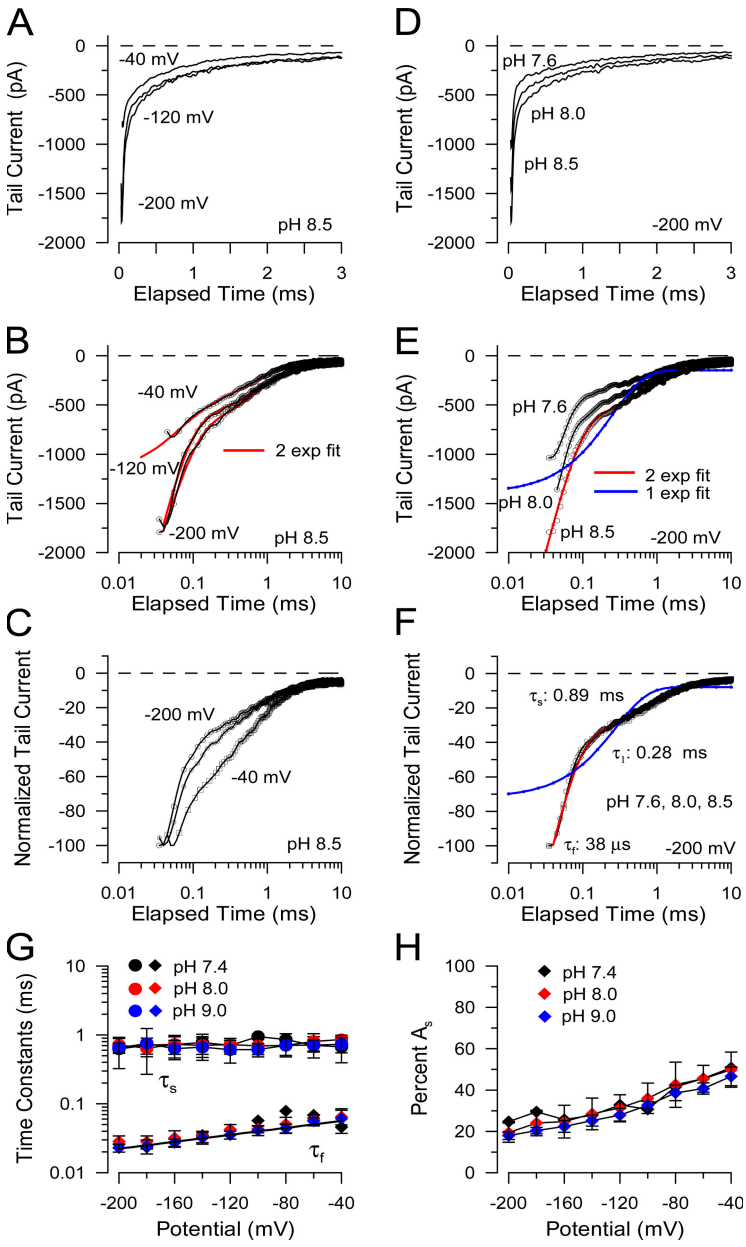


**Figure 13.** Dependence of deactivation on voltage and pH. In A, tail currents at pH 8.5 are shown on a linear time scale for −40, −120, and −200 mV. In B, traces from A are shown on a logarithmic time scale along with a two component exponential fit (red lines) to the decay process. In C, tail currents from B were normalized to their maximum amplitude to illustrate the decrease in the relative amplitude of the slow exponential component at more negative potentials. In D, tail currents at −200 mV are compared for pH 7.6, 8.0, and 8.5. In E, the traces in D are plotted on a logarithmic time scale. For the example at pH 8.5, the best fit of a single exponential function (blue line) and a two component exponential function (red line) are compared. Time constant for the single exponential fit was 0.28 ms, while for the two component fit, $\tau_f$ = 38 µs and $\tau_s$ = 0.89 ms. In F, normalized tail currents at −200 mV, but at different pH, show a similar time course. Fits are as in E. In G, slow ($\tau_s$) and fast ($\tau_f$) time constants from tail currents are plotted as a function of potential for pH 7.4, 8.0, and 9.0. For $\tau_f$, the line corresponds to $\tau_f(V) = \tau_f(0)\exp(zV/kT)$, where $\tau_f(0)$ = 0.071 ± 0.004 µs and $z$ = 0.147 ± 0.01 $e$. In H, the voltage dependence of the contribution (percent) of the slow component to the tail current is shown for pH 7.4, 8.0, and 9.0.

sensor movement ($J$) and the closed–open equilibrium ($L$). These differences account almost completely for the major differences observed in $G/V$ curves between Slo1 and Slo3. Namely, the combination of a weaker $D$ and a smaller $z_L$ underlies the following key features of Slo3 properties: (a) the pH-dependent differences in maximal conductance; (b) the low $P_o$ values at the highest voltage and pH; (c) the relatively voltage-independent steady-state conductance at negative potentials; and (d) the relatively smaller increases in relative conductance associated with movement of the voltage sensors. The smaller value for $z_J$ in Slo3 also contributes in part to the shallower $G$-$V$ in Slo3. Although we made assumptions about the magnitude both of $C$, the coupling of protonation to channel openings, and $E$, the value of coupling between the voltage sensor equilibrium and protonation, we have chosen values comparable to those used to describe Slo1. Furthermore, assumption of alternative values of $C$ and $E$ did not appreciably alter the conclusions regarding the important changes seen in $z_L$ and $D$.

### Understanding Ligand-dependent Regulation of Slo Family Channels

For Slo1, regulation by $Ca^{2+}$ primarily involves direct coupling of $Ca^{2+}$ binding to regulation of the C–O equilibrium. However, the $Ca^{2+}$ binding equilibrium does have minor effects on the voltage sensor equilibrium (Horrigan and Aldrich, 2002), and some results suggest that the effects of mM $Ca^{2+}$ and $Mg^{2+}$ may involve

Published August 28, 2006

coupling to the voltage sensor equilibrium rather than to *L* (Horrigan and Aldrich, 2002; Hu et al., 2003). Therefore, for other members of the Slo family it must be considered possible that the consequences of ligand binding as defined by Scheme 1 might involve quite different mechanisms of allosteric regulation of channel opening, perhaps involving coupling either to *L*, to *J*, or perhaps both.

Given that increases in $[H^+]$ inhibit Slo3 activation, while increases in $[Ca^{2+}]$ favor Slo1 activation, how can a structurally and functionally similar mechanism underlie regulation of both types of channel? A key point about ligand-dependent allosteric regulation is that the coupling constant between the ligand-binding equilibrium and channel regulation simply reflects the difference in ligand affinity between the closed and open channel conformations. Thus, whereas for Slo1 the open channel exhibits a high affinity for $Ca^{2+}$, for Slo3 the closed channel presumably favors protonation. In both cases, it is natural to assume that there is some conformational change that occurs in the cytosolic domains that is coupled to the status of the pore domain. A priori there is no reason why a similar sort of conformational change may not occur in both Slo1 and Slo3, but that the equilibrium is simply regulated in different directions by interaction with the ligand. The fact that chimeric constructs involving Slo1 and Slo3 work at all supports the idea that a similar underlying molecular machinery is shared (Schreiber et al., 1999; Moss and Magleby, 2001; Shi et al., 2002; Xia et al., 2004). We therefore propose that in wild-type Slo3, protonation acts on similar domains as those acted upon by $Ca^{2+}$ in Slo1 (although probably not at directly homologous residues), thereby regulating the same general conformational change.

### Differences in Voltage Dependence between Slo1 and Slo3

Recently, an intriguing study has examined the impact of all charged residues within transmembrane segments of Slo1 on estimates of $z_L$ or $z_J$ (Ma et al., 2006). One conclusion was that of a number of charged residues in S4 only one, R213, contributes directly to gating charge associated with voltage sensor movement, while other residues in S2 (D153 and R167) and S3 (D186) also contribute. Furthermore, the voltage dependence of $P_o$ and deactivation kinetics at negative potentials indicated that the same residues that influenced $z_J$ also influenced $z_L$. It was therefore proposed that the same charged residues that sense voltage during voltage sensor movement also contribute to additional motions that occur during channel opening, thus contributing to $z_L$. Given the absence of voltage dependence in $z_L$ in Slo3, but presumably smaller differences between Slo1 and Slo3 in $z_J$, comparison of charge differences between the two proteins is of interest. Surprisingly, all of the key residues thought to determine $z_J$ and $z_L$ in Slo1 are conserved in Slo3 (Fig. 14). To account for this, we imagine two possibilities. An interesting hypothesis (Ma et al., 2006) proposed to explain differences in the contributions of conserved charged residues in *Shaker* and Slo1 to gating charge was that perhaps the Slo1 voltage sensor resided in a partially activated position relative to *Shaker*. A similar idea might account for differences between Slo1 and Slo3, namely that motions of the Slo3 voltage sensor are restricted relative to Slo1. Alternatively, the differences in $z_L$ and $z_J$ between Slo1 and Slo3 may arise from differences in charged residues at other positions in transmembrane segments (Fig. 14).

### Possible Implications of the pH Dependence of Slo3 Activation Time Course

The presence of two exponential components both in the activation and deactivation time course of Slo3 contrasts markedly with Slo1. For Slo1, the single exponential time course is thought to reflect the idea that the kinetic behavior reflects a slow conformational change associated with channel opening and closing, while voltage sensor movement and $Ca^{2+}$ equilibrium steps are rapid (Horrigan and Aldrich, 2002). Although a full explanation of the basis for the kinetic behavior of Slo3 will require additional investigation, a few general comments can be made.

The primary effect of pH on Slo3 activation is to markedly change the amplitude ratio ($A_s/A_f$) of the two exponential components, while the underlying activation time constants themselves are scarcely pH dependent. What does this suggest about the underlying molecular steps in the activation process? Increases in pH result primarily in an increase in the relative contribution of the fast component of activation. It is natural, therefore, to think that protonation of the cytosolic domain somehow acts as a brake to current activation. Channels that activate at pH 7.4 do so almost exclusively with a 7–10-ms time constant, while, as the pH is increased, a larger fraction of channels opens rapidly and the absolute amplitude of the slow component of activation decreases. Yet, the relative lack of effect of pH on the underlying rates perhaps suggests that the underlying transitions do not directly involve a pH-dependent transition. To some extent, the behavior of the time constants and their relative amplitudes seems to suggest gating of two distinct, only slowly interconverting channel populations. It is as if the relative contributions of slower and faster gating components might be defined by a slow pH-dependent equilibrium established during preceding conditioning potentials. This is consistent with the observation that command voltage, per se, does not alter $A_s/A_f$, but pH does. Such a view would suggest the hypothesis that the conformation of the cytosolic module defined by its relative state of protonation determines whether a channel opens rapidly or more slowly. However, one

Published August 28, 2006

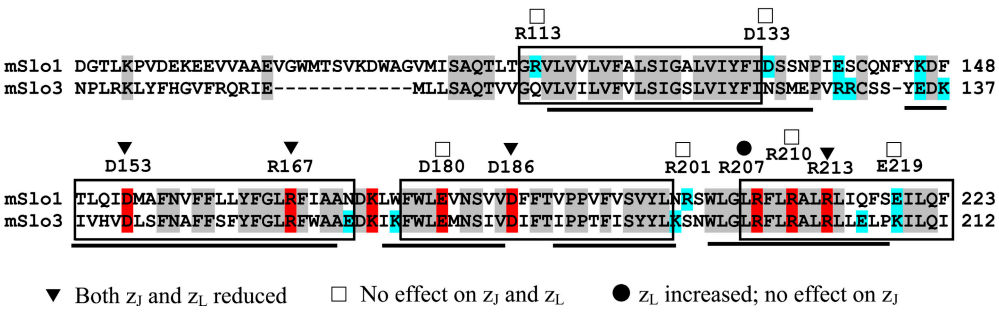


**Figure 14.** Residues implicated in voltage sensing in mSlo1 are conserved in mSlo3. Alignment compares mSlo1 and mSlo3 sequence from S1–S4. Boxed regions indicate S1–S4 defined by standard hydropathy plots, while black horizontal lines highlight putative α-helical segments defined from structural analysis (Jiang et al., 2003). Charged residues highlighted in red are identical between Slo1 and Slo3, while other identical residues are shaded in gray. Charged residues that are not conserved are highlighted in blue. All residues shown to influence both $z_J$ and $z_L$ in Slo1 (Ma et al., 2006) are conserved between Slo1 and Slo3 (▼). A number of charged Slo1 residues shown to have no effect on either $z_J$ or $z_L$ (□) are not strictly conserved in Slo3, while mutation of R207 has novel effects on $z_L$.

expectation of such a model is that channels that open through slower or faster pathways would have distinct steady-state open probabilities, and this does not appear to be observed in single channel traces (Zhang et al., 2006). Thus, at present, the information available is insufficient to propose a detailed hypothesis about the gating steps controlling Slo3 activation time course. The simplest conclusion is that multiple processes, somehow regulated by pH, contribute to the Slo3 activation time course. If slow interconversion between two relatively stable conformations is the basis for the two components of activation, it should be possible in future experiments to manipulate this behavior through appropriate variation in conditioning potentials or the duration of the conditioning steps.

### The Deactivation Behavior of Slo3 Also Contrasts Markedly with Slo1

The two components of deactivation in Slo3 also contrast with the situation in Slo1. As with the activation behavior, our current results are insufficient to provide an explanation of the two components of deactivation within the context of the allosteric model for Slo3 behavior. One complexity is the nature of the fast component of Slo3 deactivation. Our current hypothesis is that the fast component of Slo3 deactivation may be related to the flickery behavior of channel openings observed at positive potentials (Zhang et al., 2006). One curious aspect of the fast component of deactivation is that it exhibits only minimal dependence on pH. This is surprising given that the coupling of the closed–open equilibrium $L$ to the pH-dependent process might be expected to result in slowing of the channel closing process, analogous with the effect of $Ca^{2+}$ elevations on Slo1 tail currents (Zhang et al., 2001). For these reasons, we propose that the fast deactivation of Slo3 represents a novel closing process that may be unrelated to the closing of the Slo3 S6 helix. Clearly, additional work will be required to illuminate the unusual properties exhibited by this novel ion channel.

### Slo3 Current: Implications Regarding a Potential Physiological Role

The primary loci of Slo3 mRNA appears to be the testis and specifically spermatocytes (Schreiber et al., 1998), but the role of Slo3 in sperm function is unknown. As a prelude to the ability of sperm to initiate the acrosome reaction when encountering an oocyte, sperm must undergo a maturational process termed capacitance (de Lamirande et al., 1997). There is abundant evidence indicating that $Ca^{2+}$ elevations are a fundamentally important aspect of this maturational process and that the elevations of $Ca^{2+}$ occur in conjunction with or as a consequence of elevations of cytosolic pH (Santi et al., 1998; Felix, 2005). Recently, direct patch-clamp measurements have demonstrated the presence of pH-activated $Ca^{2+}$ currents in spermatocytes (Kirichok et al., 2006) most likely mediated at least in part by the CatSper1 $Ca^{2+}$-permeable, nonselective cation channel. Yet, the effectiveness of any $Ca^{2+}$ influx mechanism depends critically on the presence of a $K^+$ current to maintain gradients that support net $Ca^{2+}$ influx.

At present, the specific role of $K^+$ channels in sperm physiology remains unclear, although several candidates for $K^+$ channels important in capacitation have been proposed. One candidate is an inwardly rectifying $K^+$ current that has been recorded directly in mouse spermatogenic cells (Munoz-Garay et al., 2001) and is activated by elevations in cytosolic pH. The ability of $Ba^{2+}$ to both block this current and the sperm acrosome reaction support an important physiological role for this current. A potential role for the pH-dependent Slo3 channel in sperm physiology was also suggested with the initial cloning of this channel (Schreiber et al., 1998). However, the absence of a full functional characterization of Slo3 has placed serious limits on any speculations about its ultimate physiological role. By defining the pH and voltage dependent of Slo3 current, the present work now provides some potential insight into this issue.

One notable aspect of Slo3 current is that at pH 7.4, there is little obvious activation of voltage-dependent

Published August 28, 2006

macroscopic current even at +100 mV, and activation is only somewhat shifted to more negative potentials even at pH 8.0. As a consequence, it has been natural to wonder whether such a channel would ever contribute to plasma membrane conductances under any physiological conditions. One simple possibility is that the conditions for optimal activation of Slo3 current may not yet have been identified. Although we have a tried a number of the more obvious potential cytosolic factors, including $Na^+$, $Ca^{2+}$, $Mg^{2+}$, and 5 mM ATP (unpublished data), it certainly remains plausible that some other normal component of the cytosol may play a critical role in Slo3 regulation. However, our results establish that Slo3 currents can generate $K^+$ conductance at physiological potentials in the range of pH that occurs in spermatocytes. Specifically, because of the weak voltage dependence of the closed–open equilibrium, Slo3 channels do open at a low, but appreciable, open probability at potentials between −90 and 0 mV. Furthermore, pH changes in the range of 7.4 through 8.0 substantively regulate this open probability. As a consequence, in a cell of minimal internal volume and with sufficient numbers of Slo3 channels, the properties of Slo3 may allow it to contribute to a pH-dependent $K^+$ conductance necessary for maintenance of gradients driving $Ca^{2+}$ entry.

We thank Hai Jiang, Yimei Yui, and Yefei Cai for preparation of oocytes.

This work was supported by National Institutes of Health grant GM066215.

Lawrence G. Palmer served as editor.

Submitted: 5 April 2006
Accepted: 9 August 2006

## REFERENCES

Adelman, J.P., K.Z. Shen, M.P. Kavanaugh, R.A. Warren, Y.N. Wu, A. Lagrutta, C.T. Bond, and R.A. North. 1992. Calcium-activated potassium channels expressed from cloned complementary DNAs. *Neuron.* 9:209–216.

Avdonin, V., X. Tang, and T. Hoshi. 2003. Stimulatory action of internal protons on Slo1 BK channels. *Biophys. J.* 84:2969–2980.

Barrett, J.N., K.L. Magleby, and B.S. Pallotta. 1982. Properties of single calcium-activated potassium channels in cultured rat muscle. *J. Physiol.* 331:211–230.

Bhattacharjee, A., L. Gan, and L.K. Kaczmarek. 2002. Localization of the Slack potassium channel in the rat central nervous system. *J. Comp. Neurol.* 454:241–254.

Bhattacharjee, A., W.J. Joiner, M. Wu, Y. Yang, F.J. Sigworth, and L.K. Kaczmarek. 2003. Slick (Slo2.1), a rapidly-gating sodium-activated potassium channel inhibited by ATP. *J. Neurosci.* 23:11681–11691.

Butler, A., S. Tsunoda, D.P. McCobb, A. Wei, and L. Salkoff. 1993. mSlo, a complex mouse gene encoding "maxi" calcium-activated potassium channels. *Science.* 261:221–224.

Cox, D.H., J. Cui, and R.W. Aldrich. 1997. Allosteric gating of a large conductance Ca-activated $K^+$ channel. *J. Gen. Physiol.* 110:257–281.

Cui, J., D.H. Cox, and R.W. Aldrich. 1997. Intrinsic voltage dependence and $Ca^{2+}$ regulation of mslo large conductance Ca-activated $K^+$ channels. *J. Gen. Physiol.* 109:647–673.

de Lamirande, E., P. Leclerc, and C. Gagnon. 1997. Capacitation as a regulatory event that primes spermatozoa for the acrosome reaction and fertilization. *Mol. Hum. Reprod.* 3:175–194.

Felix, R. 2005. Molecular physiology and pathology of $Ca^{2+}$-conducting channels in the plasma membrane of mammalian sperm. *Reproduction.* 129:251–262.

Hamill, O.P., A. Marty, E. Neher, B. Sakmann, and F.J. Sigworth. 1981. Improved patch-clamp techniques for high-resolution current recording from cells and cell-free membrane patches. *Pflugers Arch.* 391:85–100.

Herrington, J., C.R. Solaro, A. Neely, and C.J. Lingle. 1995. The suppression of $Ca^{2+}$- and voltage-dependent outward $K^+$ current during mAChR activation in rat adrenal chromaffin cells. *J. Physiol.* 485:297–318.

Horrigan, F., and R. Aldrich. 2002. Coupling between voltage-sensor activation, $Ca^{2+}$ binding and channel opening in large conductance (BK) potassium channels. *J. Gen. Physiol.* 120: 267–305.

Hu, L., J. Shi, Z. Ma, G. Krishnamoorthy, F. Sieling, G. Zhang, F.T. Horrigan, and J. Cui. 2003. Participation of the S4 voltage sensor in the $Mg^{2+}$-dependent activation of large conductance (BK) $K^+$ channels. *Proc. Natl. Acad. Sci. USA.* 100:10488–10493.

Jiang, Y., A. Lee, J. Chen, M. Cadene, B.T. Chait, and R. MacKinnon. 2002. Crystal structure and mechanism of a calcium-gated potassium channel. *Nature.* 417:515–522.

Jiang, Y., A. Lee, J. Chen, V. Ruta, M. Cadene, B.T. Chait, and R. MacKinnon. 2003. X-ray structure of a voltage-dependent $K^+$ channel. *Nature.* 423:33–41.

Kirichok, Y., B. Navarro, and D.E. Clapham. 2006. Whole-cell patch-clamp measurements of spermatozoa reveal an alkaline-activated $Ca^{2+}$ channel. *Nature.* 439:737–740.

Ma, Z., X.J. Lou, and F.T. Horrigan. 2006. Role of charged residues in the S1-S4 voltage sensor of BK channels. *J. Gen. Physiol.* 127:309–328.

McManus, O.B., and K.L. Magleby. 1991. Accounting for the $Ca^{2+}$-dependent kinetics of single large-conductance $Ca^{2+}$-activated $K^+$ channels in rat skeletal muscle. *J. Physiol.* 443:739–777.

Moss, B.L., and K.L. Magleby. 2001. Gating and conductance properties of BK channels are modulated by the S9-S10 tail domain of the alpha subunit. A study of mslo1 and mslo3 wild-type and chimeric channels. *J. Gen. Physiol.* 118:711–734.

Munoz-Garay, C., J.L. De la Vega-Beltran, R. Delgado, P. Labarca, R. Felix, and A. Darszon. 2001. Inwardly rectifying $K^+$ channels in spermatogenic cells: functional expression and implication in sperm capacitation. *Dev. Biol.* 234:261–274.

Qian, X., C.M. Nimigean, X. Niu, B.L. Moss, and K.L. Magleby. 2002. Slo1 tail domains, but not the $Ca^{2+}$ bowl, are required for the beta 1 subunit to increase the apparent $Ca^{2+}$ sensitivity of BK channels. *J. Gen. Physiol.* 120:829–843.

Rothberg, B.S., and K.L. Magleby. 1999. Gating kinetics of single large-conductance $Ca^{2+}$-activated $K^+$ channels in high $Ca^{2+}$ suggest a two-tiered allosteric gating mechanism. *J. Gen. Physiol.* 114:93–124.

Rothberg, B.S., and K.L. Magleby. 2000. Voltage and $Ca^{2+}$ activation of single large-conductance $Ca^{2+}$-activated $K^+$ channels described by a two-tiered allosteric gating mechanism. *J. Gen. Physiol.* 116:75–99.

Santi, C.M., T. Santos, A. Hernandez-Cruz, and A. Darszon. 1998. Properties of a novel pH-dependent $Ca^{2+}$ permeation pathway present in male germ cells with possible roles in spermatogenesis and mature sperm function. *J. Gen. Physiol.* 112:33–53.

Schreiber, M., and L. Salkoff. 1997. A novel calcium-sensing domain in the BK channel. *Biophys. J.* 73:1355–1363.

Published August 28, 2006

Schreiber, M., A. Wei, A. Yuan, J. Gaut, M. Saito, and L. Salkoff. 1998. Slo3, a novel pH-sensitive $K^+$ channel from mammalian spermatocytes. *J. Biol. Chem.* 273:3509–3516.

Schreiber, M., A. Yuan, and L. Salkoff. 1999. Transplantable sites confer calcium sensitivity to BK channels. *Nat. Neurosci.* 2:416–421.

Shi, J., G. Krishnamoorthy, Y. Yang, L. Hu, N. Chaturvedi, D. Harilal, J. Qin, and J. Cui. 2002. Mechanism of magnesium activation of calcium-activated potassium channels. *Nature.* 418:876–880.

Sigg, D., and F. Bezanilla. 1997. Total charge movement per channel. The relation between gating charge displacement and the voltage sensitivity of activation. *J. Gen. Physiol.* 109:27–39.

Wei, A., C. Solaro, C. Lingle, and L. Salkoff. 1994. Calcium sensitivity of BK-type KCa channels determined by a separable domain. *Neuron.* 13:671–681.

Xia, X.M., J.P. Ding, and C.J. Lingle. 1999. Molecular basis for the inactivation of $Ca^{2+}$- and voltage-dependent BK channels in adrenal chromaffin cells and rat insulinoma tumor cells. *J. Neurosci.* 19:5255–5264.

Xia, X.-M., X.-H. Zeng, and C.J. Lingle. 2002. Multiple regulatory sites in large-conductance calcium-activated potassium channels. *Nature.* 418:880–884.

Xia, X.-M., X. Zhang, and C.J. Lingle. 2004. Ligand-dependent activation of Slo family channels is defined by interchangeable cytosolic domains. *J. Neurosci.* 24:5585–5591.

Yuan, A., C.M. Santi, A. Wei, Z.W. Wang, K. Pollak, M. Nonet, L. Kaczmarek, C.M. Crowder, and L. Salkoff. 2003. The sodium-activated potassium channel is encoded by a member of the Slo gene family. *Neuron.* 37:765–773.

Zeng, X.-H., X.-M. Xia, and C.J. Lingle. 2001. Gating properties conferred on BK channels by the β3b auxiliary subunit in the absence of its N and C termini. *J. Gen. Physiol.* 117:607–627.

Zhang, X., C.R. Solaro, and C.J. Lingle. 2001. Allosteric regulation of BK channel gating by $Ca^{2+}$ and $Mg^{2+}$ through a non-selective, low affinity divalent cation site. *J. Gen. Physiol.* 118:607–635.

Zhang, X., X.-H. Zeng, X.M. Xia, and C.J. Lingle. 2006. pH-regulated Slo3 $K^+$ currents: properties of unitary currents. *J. Gen. Physiol.* 128:301–315.